



**Deliverable 2.18: Model abstraction methods for upscaling and integration of process knowledge in reactive transport models for geological disposal of radioactive waste**

Work Package [ACED](#)

This project has received funding from the European Union's Horizon 2020 research and innovation programme under grant agreement N 847593.



## Document information

Project Acronym	<b>EURAD</b>
Project Title	<b>European Joint Programme on Radioactive Waste Management</b>
Project Type	<b>European Joint Programme (EJP)</b>
EC grant agreement No.	<b>847593</b>
Project starting / end date	<b>1<sup>st</sup> June 2019 – 30 May 2024</b>
Work Package No.	<b>2</b>
Work Package Title	<b>Assessment of Chemical Evolution of ILW and HLW disposal cells</b>
Work Package Acronym	<b>ACED</b>
Deliverable No.	<b>2.18</b>
Deliverable Title	<b>Model abstraction methods for upscaling and integration of process knowledge in reactive transport models for geological disposal of radioactive waste</b>
Lead Beneficiary	<b>SCK CEN</b>
Contractual Delivery Date	<b>M24</b>
Actual Delivery Date	<b>M32</b>
Type	<b>Report</b>
Dissemination level	<b>Public</b>
Authors	<b>Joan Govaerts (SCK CEN), Diederik Jacques (SCK CEN), Javier Samper (UDC), Erika Neeft (COVRA), Vanessa Montaya (UFZ)</b>

### To be cited as:

Govaerts J., Jacques D., Samper J., Neeft E., Montaya V. (2022): Model abstraction methods for upscaling and integration of process knowledge in reactive transport models for geological disposal of radioactive waste. Final version as of 10.01.2022 of deliverable D2.18 of the HORIZON 2020 project EURAD. EC Grant agreement no: 847593.

### Disclaimer

All information in this document is provided "as is" and no guarantee or warranty is given that the information is fit for any particular purpose. The user, therefore, uses the information at its sole risk and liability. For the avoidance of all doubts, the European Commission has no liability in respect of this document, which is merely representing the authors' view.

### Acknowledgement

This document is a deliverable of the European Joint Programme on Radioactive Waste Management (EURAD). EURAD has received funding from the European Union's Horizon 2020 research and innovation programme under grant agreement No 847593.

Status of deliverable		
	By	Date
Delivered (Lead Beneficiary)	SCK CEN	2021-08-25
Verified (WP Leader)	Diederik Jacques (SCK CEN)	2021-08-31
Reviewed (Reviewers)	Jacques Wendling (ANDRA)	2021-10-22
	Francis Claret (BRGM)	2021-11-15
	Hans Meeussen (NRG)	2021-10-25
Verified (WP Leader)	Diederik Jacques (SCK CEN)	2022-01-10
Approved (PMO)	Louise Théodon (ANDRA)	2022-01-10
Submitted to EC (Coordinator)	ANDRA	2022-01-10

## Executive Summary

Reactive transport models in the context of radioactive waste disposal tend to become increasingly complex due to advancements in understanding and quantifying of (geo)chemical and transport processes in the engineered barriers and surrounding geological layers.

The complexity of these models is caused by the large number and intricacies of the simulated processes, number of interacting species and/or components, differences in scales at which the interactions occur and amount of couplings to simulate. The models can become even more challenging as they have to be applied to long timescales and large spatial scales.

Many model abstraction techniques have been developed in the last decades and the state of the art is described in this document. Several techniques are explained together with comprehensive descriptions of a plethora of case studies.

Performing model abstractions will likely result in many benefits. It will foremost improve the understanding of the complex models and (the role of) their essential factors. This again will aid to communicate the modelling results to both a technical and lay public. The reduced computational burden of the model can lead to a more robust uncertainty and sensitivity analysis, which in turn will build the confidence in the model predictions.

## Table of content

Executive Summary.....	4
Table of content.....	5
List of figures .....	7
List of Tables .....	10
1. Introduction .....	11
2. Model abstraction.....	12
2.1 General definition of model abstraction .....	12
2.2 Rationale for model abstraction for reactive transport in the context of radioactive waste disposal .....	12
2.3 Procedure for Model abstraction.....	13
3. Model abstraction techniques .....	14
3.1 Lower-fidelity physically-based modelling.....	16
3.1.1 Hierarchy of models .....	16
3.1.2 Delimited input domain .....	21
3.1.3 Scale change .....	31
3.1.4 Reduced numerical accuracy.....	33
3.2 Response surface surrogate modelling or Meta-modelling.....	34
3.2.1 Meta-modelling on full reactive transport models.....	35
3.2.2 Meta-models used to replace the geochemical solver .....	35
3.2.3 Meta-models used as replacement of process models .....	37
3.2.4 Meta-modelling in DONUT .....	40
4. Discussion.....	42
5. Conclusion .....	43
6. Appendix A: Reduced numerical accuracy: impact of mesh size .....	45
6.1 Context.....	45
6.2 Example cementitious material.....	45
6.2.1 Transport of water .....	45
6.2.2 Transport of water and reactive gas.....	48
7. Appendix B: Reduced complexity and impact of discretization and convergence tolerance.....	50

## EURAD Deliverable ACED 2.18 – Model abstraction techniques

7.1	Introduction.....	50
7.2	Sensitivity of computed Cs concentrations to the convergence tolerance for solving the geochemical equations.....	50
7.3	Conclusions.....	51
8.	Appendix C: Reduced dimensionality in axi-symmetric models .....	54
8.1	Introduction.....	54
8.2	Febex in situ test .....	54
8.3	1D and 2D axi-symmetric models for a HLW repository in granite .....	60
	References .....	64

## List of figures

Figure 3-1: Model abstraction methods - classification .....	15
<i>Figure 3-2: Conceptual models of a fractured porous medium. The placements of the different models relative to each other depend on the original fractured porous medium, to which extent scale separation exists, and on the applied modelling choices and upscaling procedures as well as the available information on the original medium. For example, if a DFM model represents all fractures of the original medium, it is a perfect model with the same placement as the original medium in the illustration. The same is true for the single-continuum model in the special situation where an REV exists (taken from [7]).</i> .....	18
Figure 3-3: Portlandite volume fraction (–) after 50 000 years: comparison of the results of the 3D compartment-scale model (left) and the 2D simulation (right), taken from [23]. .....	22
Figure 3-4: a) A 1D continuum is embedded in a 3D grid that occupies the X, Y, and Z dimensions. b) The 1D continuum occupies a virtual 4th dimension; one end of the 1D continuum coincides in space with a cell center in the 3D grid. c) Cell volumes and connection areas within the 1D continuum represent concentric shells of a cylindrical volume occupying the volume of the connected 3D cell, taken from [24]. .....	23
Figure 3-5: Computational grid: (top) excerpt of two-dimensional, vertical cross-section of the three-dimensional Voronoi grid of the geosphere; (bottom) excerpt of radial-axial grid of near-field; the radial-axial grid of the near-field model follows the trajectory of the drillhole and is embedded in the Cartesian grid of the geosphere model. All computational cells of the near-field model are ring-shaped annular grid blocks. The radial discretization is shown on the rightmost cross section; interface radii conform to material interfaces between waste, canister, backfill, casing, cement, excavation disturbed zone (EDZ), and host rock. Outside the maximum radius shown here, the host rock is discretized using logarithmically increasing interface spacings up to a radius of 10 m, at which point the radial-axial grid is connected to the three-dimensional Voronoi grid of the geosphere, taken from [26]. .....	24
Figure 3-6: Physical representation of the system comprising two reservoirs and the synthetic fracture network in the framework of a) the discrete model and b) the equivalent porous media model, taken from [58] .....	33
Figure 3-7: <i>Dissolved Calcite (mol). (a) End of CO<sub>2</sub> injection period. (b) End of simulation with geochemical solver. (c) End of simulation with ANN, taken from [69].</i> .....	37
<i>Figure 3-8: Comparison of look-up table approach (MP-LT) and full reactive transport model (GEM): pH and porosity profiles at different times in the carbonation benchmark case. The right side of the simulation domain at 1 m is a closed boundary, taken from [58].</i> .....	39

Figure 3-9: Comparison of the solid Ca profiles and the ends of chemical degradation state II and III between the full and abstracted model during diffusive transport conditions, taken from [75]..... 40

Figure 6-1: Calculated weight of water in the cubical samples for exposed to a relative humidity of 75% and 43% at different mesh densities. .... 46

Figure 6-2: Simulated with an extremely fine mesh, diffusion values for water in samples of COVRA’s waste package as a function of time during exposure to a relative humidity of 43% and 75%. Range in linear scale: maximum  $5.3 \times 10^{-12}$  m<sup>2</sup>/s (dark red), minimum  $5.3 \times 10^{-15}$  m<sup>2</sup>/s (dark blue). .... 47

Figure 6-3: Simulated with an extremely fine mesh, saturation degrees in samples of COVRA’s waste package mortar as a function of time during exposure to a relative humidity of 43% and 75%. Range in linear scale: maximum 1 (dark red), minimum 0 (dark blue). .... 48

Figure 6-4: Predicted disappearance of pyrite as a function of time for a normal mesh and extremely fine mesh for initially water saturated samples that were when exposed to a relative humidity of 54%. Range in linear scale: maximum 9.6 mol FeS<sub>2</sub>/m<sup>3</sup> (dark blue), minimum 0 (white). .... 49

*Figure 7-1: Sensitivity analysis of the time evolution of the Cs concentrations computed with CORE<sup>2D</sup>V5 at  $x = 1$  mm (top) and at  $x = 5$  mm (bottom) by using different relative convergence tolerance ( $\omega$ ) to solve the chemical reactions. The cesium concentration at the “high” concentration boundary is equal to  $10^{-7}$  mol/L [78].*..... 51

*Figure 7-2: Cs breakthrough curves calculated with the multi-species transport models at different locations in the Opalinus clay samples by using five reactive transport codes. The cesium concentration at the “high” concentration boundary are equal to  $10^{-3}$  mol/L (top),  $10^{-5}$  mol/L (middle) and  $10^{-7}$  mol/L (bottom).* ..... 52

Figure 8-1: General layout of the FEBEX in situ test, taken from [80]. .... 54

Figure 8-2: Time evolution of the calculated temperatures (lines) with the 1D and 2D axisymmetric models and the measured temperatures (symbols) in a hot section at radial distances  $r = 0.48$  m,  $r = 0.82$  m and  $r = 1.05$  m taken from [79]. .... 56

Figure 8-3: Time evolution of the computed water content (lines) with the 1D and 2D axisymmetric models and measured data (symbols) in a hot section taken from [79]. ..... 57

Figure 8-4: Contour plots of the computed Cl<sup>-</sup> concentrations at dismantling times of Heater #1 in 2002 (left) and Heater #2 in 2015 (right) taken from [79]. .... 59

Figure 8-5: Geometry and material zones of the 2-D axisymmetric model (top) and zoom of the canister-bentonite-EDZ (bottom) taken from [82]. .... 61

Figure 8-6: Finite element mesh used in the 1-D axisymmetric model [82]. .... 61

Figure 8-7: Computed spatial distribution of the cumulative canister corrosion and magnetite precipitation after  $10^5$  years (top) and  $2 \cdot 10^5$  years (bottom) (units: mol/L) [82]. ..... 63

Figure 8-8: Sensitivity of the computed  $\text{Cl}^-$  concentration of dissolved  $\text{Cl}^-$  in the bentonite ( $r = 0.8$  m) to groundwater flow. It should be noticed that 2-D model with no flow and the 1-D model provide identical results [82]. ..... 63

## List of Tables

Table 1: Mesh characteristics for cubical samples with an edge of 5 cm and computational time for non-linear diffusion of water (% indicates relative humidity). 45

## 1. Introduction

Numerical simulation models, which represent physical systems by using mathematical concepts, are often playing a key role in engineering tasks and decision making processes.

On the one hand, modern simulation models tend to become more and more computationally intensive as the improving scientific knowledge about the real-world systems is increasingly better and computing power allows it to be inserted in the model.

On the other hand, safety assessment and supporting models in the context of radioactive waste disposal often need to be relatively simple and/or fast to allow computations for large scales and extremely long time scales, or to execute it many times with different parameters for sensitivity and uncertainty analysis.

This raises the need for model abstraction (MA). This is defined as the methodology for reducing the complexity or the computational burden of a simulation model while maintaining the validity of the simulation results with respect to the question that the simulation is being used to address [1].

One possibility is to develop and verify lower-fidelity physically based models which would be able to reproduce the most important features of the ‘higher-fidelity’ complex model. These lower-fidelity (or abstracted) models are simplified from so-called high-fidelity models (e.g. dimensionality, geometry, transport or geochemical processes, parameterization) in such a way that the key output of interest obtained with the abstracted model are acceptable in terms of accuracy and computational resources with respect to the original model [1].

Another possibility to lift some of the computational burden is to develop and use cheaper-to-run response surface surrogates of the “original” simulation models. Response surface surrogates employ data-driven function approximation techniques to emulate the model input-output relations. Response surface surrogates may also be referred to as “metamodels” as a response surface surrogate is a “model of a model” [2].

This report deals specifically with model abstraction for reactive (coupled) transport modelling in the context of radioactive waste disposal, which in practice are often the most challenging and demanding type of models used in this research area.

Chapter 2 gives a general definition of model abstraction and discusses the rationale and workflow behind it.

In chapter 3, several techniques are explained, together with comprehensive descriptions of a plethora of case studies. These are subdivided in two large classes: the lower-fidelity physically based models and the Response surface surrogate models.

After chapters 4 and 5, respectively, a discussion and concluding remarks, additional case studies and worked examples are given in appendices A-C.

## 2. Model abstraction

### 2.1 General definition of model abstraction

Model abstraction (MA) is defined as the methodology for reducing the complexity or the computational burden of a simulation model while maintaining the validity of the simulation results with respect to the question that the simulation is being used to address [1]. In a recent study [3], the authors investigated the geoscientific community's understanding of model complexity. Their survey shows that there is “no general consensus on how model complexity is perceived or should be defined.” However, 78% of the participants consider the “number of processes explicitly included” as an adequate characterization of model complexity, followed by the “number of interactions/feedback incorporated.” It must be noted that depending on the desired output of the simulation, different abstracted models can be developed in order to address different questions.

Model abstraction reduces the simulated system to its essential components and processes through a simplification of conceptual (sub)models, selection of significant processes and appropriate time and spatial scales or more computationally efficient implementations (of specific model components and processes). In its most extreme form, the model is stripped down to a single component which just reproduces the desired output from the input in a computationally more efficient way (so-called meta-models, see §3.2.1).

### 2.2 Rationale for model abstraction for reactive transport in the context of radioactive waste disposal

Reactive transport models in the context of radioactive waste disposal tend to become increasingly complex due to advancements in understanding and quantifying of (geo)chemical and transport-processes in the engineered barrier systems and surrounding geological layers [4]. The complexity of these models is caused by the large number and intricacies of the simulated processes, many interacting species and/or components, differences in scales at which the interactions occur and amount of feedbacks to simulate. Indeed, most physical and chemical phenomena can be either weakly or strongly coupled and may vary in time and space scales. Additionally, due to the long timescales ( $>10^4$  years) and large spatial scales (up to several tens of m) involved, the resolution of these models can become even more challenging.

The uncertainty that by default is associated with the model structure, along with the data and scenario uncertainty, is known to introduce large uncertainties in the modelling results. To partially cope with this, tens if not hundreds of simulations would have to be executed to perform a decent uncertainty and sensitivity analysis [5].

Moreover, an excessive burden of data collection can be expected in order to correctly parametrize the input requirements of the model. Furthermore, difficulties could arise in interpreting complex and high-dimensional simulation results and conveying the

simulation output to both technical and lay audiences. This might necessitate the need to revert the high-fidelity model to a more plain and uncomplicated form, for instance to permit a more thorough analysis for a given analysis budget.

One can view the model abstraction procedure as a form of simplification of the (execution of the) model that assures validity of the model for the specific purpose. The model abstraction implementation has to ensure objectiveness and comprehensiveness of the resulting model. By a transparent step-by-step and traceable implementation and its reporting, one should be able to justify and verify the use of the simplified or abstracted model.

### 2.3 Procedure for Model abstraction

The MA process starts with an existing (high-fidelity) *base* model. The *key output* of the model is defined so it provides the necessary information to decide on issues of interest. It must be noted, that this high-fidelity model might have already some simplifications/abstractions by default as an unacceptable resource demand of the base model might even preclude the feasibility and completion of the modelling project.

The model abstraction process should include the following steps:

- Justify the need for the model abstraction
  - Before actually performing the model abstraction, one should investigate the feasibility of that particular work, by judging on the resources spent on pre-processing, calibration, verification/post-processing and reporting of the abstraction work. It is important to try to estimate the gain in computational speed from the abstraction, as well as human resources available to perform and document the abstraction process. This should be compared to the time and expenses needed for executing and interpreting the original base model.
- Review the context of the modelling problem
  - The context of the modelling problem has to be reviewed to assure the objectiveness and the comprehensiveness of the model abstraction. It needs to be realized what details and features of the problem are omitted or de-emphasized when the abstraction is performed.
- Select applicable MA techniques and ‘simplify’ model where feasible
- Perform verification calculations to ensure the abstracted model performs well within the conditions where it is derived from. as they are (probably) only valid within these ranges. Care must be taken when those models are used for extrapolations or when coupled to additional physical models.
- Report the justification, abstraction process and verification in a traceable and transparent way.
- Reap the benefits of the abstraction
  - Perform extensive sensitivity and uncertainty analysis, either local or global
  - E.g. use the reduced geo-chemical (meta-)model on a larger spatial and dimensional scale

### 3. Model abstraction techniques

The classification of MA techniques is based on a combination of the classifications proposed by [6] and [2]. We will distinguish between two broad families under the large umbrella of model abstraction techniques: (1) lower-fidelity physically-based modelling and (2) response surface surrogates (or meta-modelling).

The construction of **lower fidelity (reactive flow and transport) numerical models** with model abstraction can be done by one or more of following strategies: (a) using pre-defined hierarchies of models, (b) delimiting the input domain, (c) scale change done by either upscaling or aggregation and (d) reducing numerical accuracy.

A predefined *hierarchy* contains a series of progressively more simple conceptual and corresponding mathematical representations of flow and (reactive) transport and geochemical reactions in porous media (§3.1.1). For instance, reducing the complexity of the transport model can free up computational resources for the geochemical system calculations, if this is deemed more relevant for the questions at hand.

The class of model abstraction techniques based on the *delimiting input domain* utilises the fact that some features, events, or processes may be not relevant for a given set of scenarios or for a given set of model outputs (§3.1.2). In practice, this will often result in a lower dimensionality of the problem, for instance by effectively using less spatial dimensions, or lowering the complexity of the geochemical system.

*Scale change* provides transitions between different operational scales (§3.1.3). Model abstraction with scale change alters model equations, variables and parameters with two classes of methods: upscaling and aggregation. Upscaling model abstraction methods use the fine-scale model and the fine-scale media properties to derive the coarse-scale model equations and to relate the coarse-scale and fine-scale transport parameters. Unlike in upscaling, for aggregation no relationship is assumed between model parameters at the fine and at the coarse scales. Parameters of the coarse-scale model are lumped by combining several materials.

*Reducing numerical accuracy* (§3.1.4) results in lower-fidelity models which are fundamentally the same as the original models. For example, a lower-fidelity model can be a variation of the original model but with larger (coarser) spatial/temporal grid size.

**Response surface surrogates or Metamodeling** (§3.2) seek to simulate the input-output relationships of the complex model with a statistical relationship without taking the underlying physics into account (i.e. black box models). Meta-models can be used to emulate the full reactive transport model (§3.2.1), to replace the solver of the geochemical step in reactive transport codes (§3.2.2) and to replace computationally expensive process models (§3.2.3).

The next sections present a systematic description of the model abstraction techniques. Each section includes a short description of the method class, some general examples of application of the method, and a more in-depth discussion of case studies which are more relevant to the modelling of the chemical evolution in radioactive waste disposal cells. If possible, potential application in ACED models is discussed, together with the pros and cons of each method.

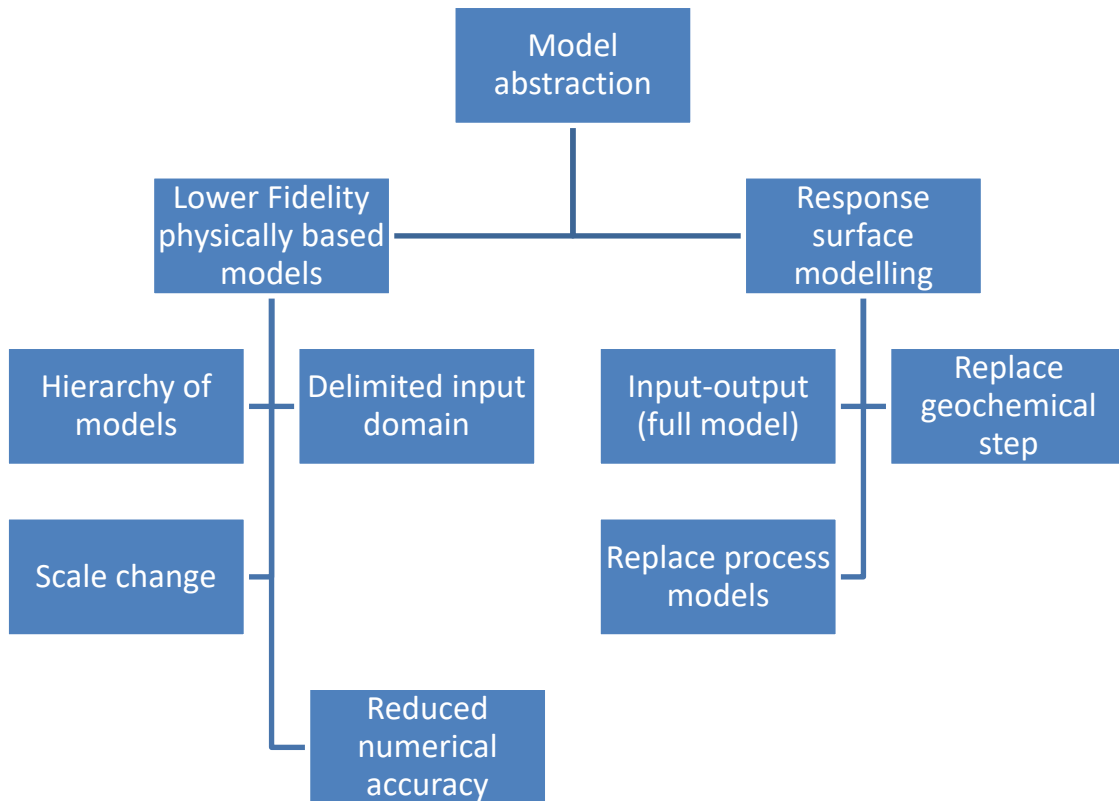


Figure 3-1: Model abstraction methods - classification

### 3.1 Lower-fidelity physically-based modelling

#### 3.1.1 Hierarchy of models

A predefined hierarchy contains a series of progressively more simple conceptual and corresponding mathematical representations of flow and/or transport in porous media. A nice illustration of this can be found in the research field of fractured porous media flow and transport [7].

##### 3.1.1.1 FLOW AND TRANSPORT

###### CASE STUDY: FLOW AND TRANSPORT IN FRACTURED POROUS MEDIA

Figure 3-2 shows a schematic representation of increasingly complex models that may be used in these type of media.

The simplest approach is the single-continuum approach and use Richards equations for variably-saturated water flow and the advection-dispersion equation for solute transport. In single-continuum flow models, the fractures are represented by adapting the permeability of the porous medium. The permeability may increase or decrease, and the orientation of the tensor may change depending on the properties of the fractures and the fracture network. In terms of discretization, single-continuum models are by far the most convenient: At any point in space, there is a single value for each parameter such as permeability and porosity. However, the simplicity of the conceptual model comes with the burden of finding appropriate effective parameters. This can be a challenging task, especially when there is no Representative Elementary Volume (REV) to be found due to different length scales of the porous matrix, micro- and/or macrofractures (so-called lack of scale separation). As such, the effective parameters can be length-scale specific as they should account for inherent properties of the fractures themselves such as orientation, aperture, surface roughness,... as well as properties of the fracture network such as fracture density [8]. Additionally, dynamics and local detail are often not adequately represented by averaged flow and transport alone.

A next level of sophistication are the so-called multi-continuum approaches. These are families of methods that represent the fractured porous medium by several superimposed media with their own conservation equations and constitutive laws. The simplest approach consists of a fracture continuum and a matrix continuum and is referred to as dual-continuum model. An extension to a general number of continua can account for heterogeneities in properties within the fracture/matrix continuum. For each included medium, the number of degrees of freedom increases significantly. This can substantially increase the computational cost of the simulation.

The main challenge of multi-continuum modelling is defining the transfer term. This represents the transfer rate of water, heat and/or solutes between the different continua. In order to be predictive, its parameters should be derived from geometrical, topological and physical properties of the individual continua. The only physical constraint is mass conservation. In one of the first formulations of the transfer term (within the double porosity method as originally proposed by [9]), the rate of inter-

porosity flow is proportional to the local difference in average pressures between fractures and matrix, which is acceptable in the case of a rapid transient response of the matrix.

When this assumption is not valid, e.g. in the case of non-isothermal and multiphase flow, this can be overcome by expanding the matrix continuum into a series of multiple interacting continua (MINC, as implemented in TOUGH2, see [10]). The MINC method treats inter-porosity flow in a fully transient way by computing the gradients which drive inter-porosity fluxes at the matrix-fracture interface. A similar approach, yet computationally more efficient, is implemented in PFLOTRAN [11]. It uses a highly efficient algorithm as the primary and secondary continua are solved separately treating the secondary continua as a 1D system of equations. This method is referred to as the Dual Continuum Disconnected Matrix (DCDM) and was recently benchmarked to several reactive transport test cases [12]. The authors showed that if the DCDM is implemented with a careful grid spacing, particularly at the interface between primary and secondary continuum, it can accurately capture matrix diffusion processes along with chemical reactions in reactive transport modelling of fractured rocks.

Multi-rate Mass transfer (MRMT) models [13] have been developed as an extension of MINC for porous media in diffusive conditions. These are referred to as Structured INTERacting Continua (SINC, [14]). Here, a structure in the immobile domain is introduced, coming for example from the dead-ends of fracture clusters or poorly-connected dissolution patterns. These MRMT models are shown to accurately approach transport in structured diffusion-dominated porous structures at intermediate and long times and only miss early responses.

The modelling approach can be refined further by modelling the fractures and matrix as separate geometric objects. Depending on the specific approach being employed, this reduces or even removes the need to represent flow by upscaled quantities. As such, modelling with explicit representation of fractures is often conceptually simpler than the implicit counterpart (single – and multi-continuum approaches), but at the cost of dealing with complex geometries. The network of fractures is referred to as a discrete fracture network (DFN). By analogy, models that ignore flow in the porous medium, or consider it impermeable, are referred to as Discrete fracture networks models. In a DFN model, all fluid is assumed to be contained within the fracture network.

Additional complexity can be introduced by considering transient flow and/or transport in discrete fractures with interactions between the fractures and matrix. This approach is based on the assumption that the flow and transport equations of the fracture network can be solved in a fully coupled fashion with corresponding equations for the matrix and is referred to as Discrete fracture matrix (DFM) modelling ([15]). DFM models often balance between loss of accuracy by upscaling and geometric complexity. Not all fractures can be treated explicitly and some need to be considered as part of the porous matrix by averaged quantities.

Quantitative comparisons between a number of different numerical approaches are presented for DFM models by [16], DFN models by [17] and DFM and dual-continuum models by [18].

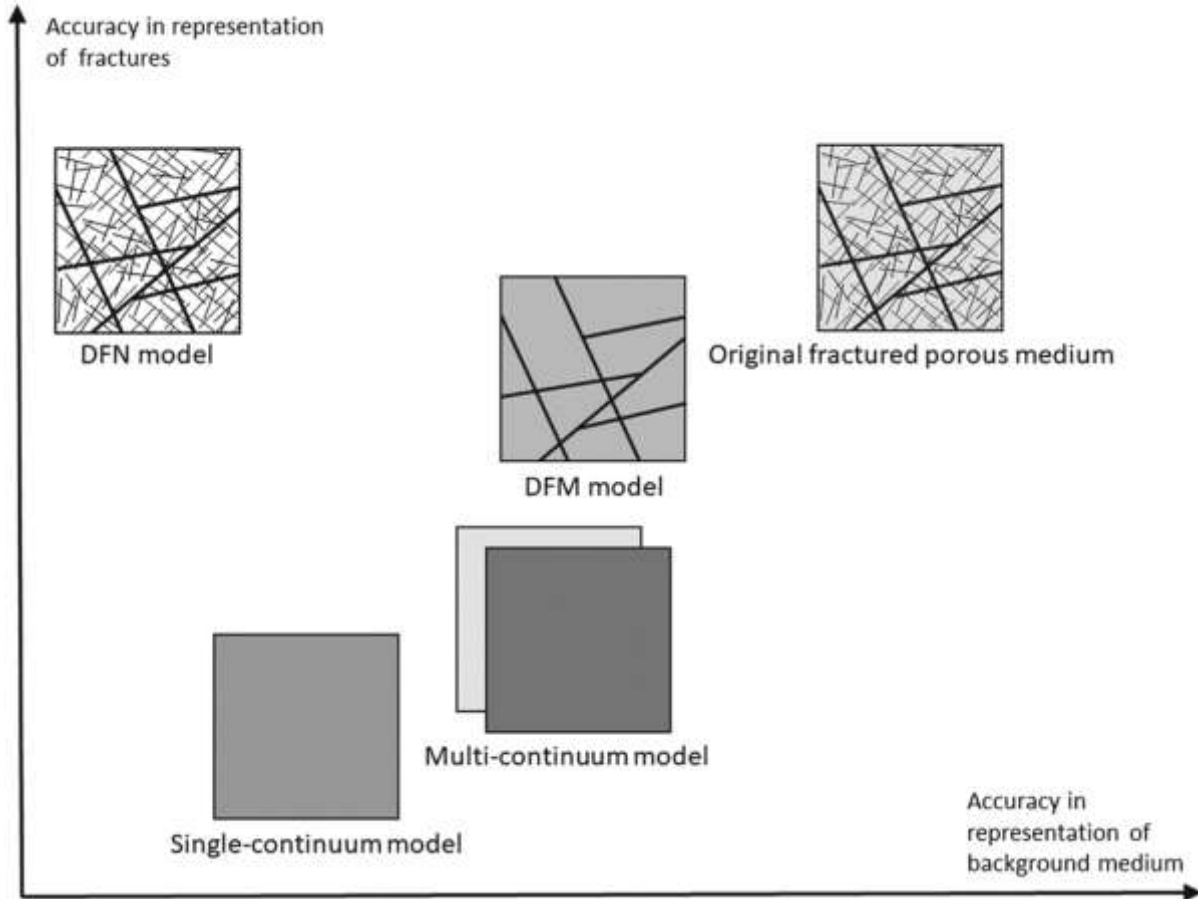


Figure 3-2: Conceptual models of a fractured porous medium. The placements of the different models relative to each other depend on the original fractured porous medium, to which extent scale separation exists, and on the applied modelling choices and upscaling procedures as well as the available information on the original medium. For example, if a DFM model represents all fractures of the original medium, it is a perfect model with the same placement as the original medium in the illustration. The same is true for the single-continuum model in the special situation where an REV exists (taken from [7]).

## CASE STUDY: DIFFUSION IN CHARGED POROUS MEDIA

The review article of [19] gives an overview of different models and conceptualisations for diffusive (and advective) transport in charged nanoporous materials. Clays, which are comprised of an assembly of layered minerals, are by far the most studied of these materials. Isomorphic substitutions by cations of lower charge in these layered structures result in a negative layer charge. The charge of the surfaces bordering the pores is responsible for the presence of a double layer or electrical double layer (EDL), i.e., the layers of interfacial water and electrolyte ions.

The Poisson–Boltzmann (PB) equation relates the local charge imbalance at a position in the direction perpendicular to the charged surface to the second derivative of the electrostatic potential at the same position which allows to calculate distribution of ions in the EDL (and more specific its diffuse layer).

In practice, the information about ion concentrations in the diffuse layer must be upscaled so that calculations can be carried out at the continuum scale. As the solution of the PB equation for multiple species and in complex porous structures is not straightforward, a common upscaling approach relies on the use of a mean electrostatic potential (MEP) model, often referred as a Donnan model in the literature. This model averages ion concentrations in the diffuse layer by scaling them to a mean electrostatic potential. In general, the approximation is good, but the accuracy of the MEP model predictions degrades as the size of the pore increases and as the ionic strength of the solution decreases.

This information can be used to construct a so-called dual continuum model. The mean electrostatic potential model can be adapted to do so, following the basic principle of a subdivision of the pore space into two compartments, one being electroneutral, and the other being influenced by a non-zero mean electrostatic potential value.

The most complex formulation for multi-component (MC) diffusion in charged media is the Nernst-Planck (NP) equation, which is based on the conservation of the electrochemical potential. Reactive transport codes such as PHREEQC, ORCHESTRA and CrunchClay are able to solve NP Equation under transient and stationary conditions with a diffuse layer dual continuum model.

In [20] a nice demonstration of this lower-fidelity physically-based modelling is presented. A workflow was developed to replace computationally intensive multicomponent uranium diffusion simulations based on the Nernst-Planck formulation with single component (SC) Fickian diffusion models.

MC diffusion simulations were calibrated on the metre-scale and transposed to the host rock scale (far-field) and a simulation time of one million years. For that, the authors used a distribution coefficient and an effective diffusion coefficient, that was calibrated for shaly, sandy and carbonate-rich facies of the Opalinus Clay. On the host rock scale, the MC simulations required a computing time between 5 h and 6 h, whereas the SC simulations were done in a few seconds. The application to the host rock scale was evaluated by comparison with a representative MC simulation for each

facies and for a simulation time of one million years. The MC simulations could be reproduced on the host rock scale with the transport parameters calibrated on the small scale with a deviation between 2% and 4%.

### 3.1.1.2 (GEO)CHEMISTRY

#### CASE STUDY: URANIUM SORPTION [21]

The objective of this study was to test if a simpler, semi-empirical, non-electrostatic U(VI) sorption model (NEM) could achieve the same predictive performance as a surface complexation model (SCM) with electrostatic correction terms in describing U(VI) plume evolution and long-term mobility. One-dimensional reactive transport simulations considering key hydrodynamic processes, Al and Fe minerals, as well as H<sup>+</sup> and U surface complexation, with and without electrostatic correction terms, were conducted. A key finding of this study is that the applicability of NEM (and thus robustness of its predictions) to the field system evolves with time and is strongly dependent on the pH range that was used to develop the model.

#### CASE STUDY: LINER DEGRADATION IN CONTACT WITH CLAY-ROCK

The objective of this work [22] was to study the interaction between a newly-developed low-pH concrete and a clay host rock (i.e. Callovo Oxfordian) over 100,000 years. The main goal was to build confidence in the consistency of the different modelling approaches implemented in different reactive transport codes (iCP, ORCHESTRA, OpenGeosys-GEM, CORE2D, and MIN3P) by using a common reference case. The base case was a complex mechanistic reactive transport model including precipitation/dissolution reactions, redox and cation exchange processes. In addition, sensitivity cases were simulated to test the effect of considering some additional geochemical and coupled transport processes. The additional processes included a) the impact of porosity changes on the diffusion coefficient b) kinetic dissolution of clays and b) electrochemical couplings. The sensitivity cases modelled showed that the results obtained were very sensitive to the different couplings used between porosity and diffusivity (i.e from linear to more complex relationships). The impact of including or not the slow kinetics of dissolution of the claystone minerals was shown to be negligible in the studied scenarios. On the other hand, although the effect of the electrochemical coupling was clearly visible, the impact of the evolving electric potential gradients on the effective ion diffusion rates was small

### 3.1.2 Delimited input domain

This class of model abstraction techniques relies on the fact that some processes, features or parameters may be not relevant or have an insignificant impact for a given class of scenarios or for a given set of model outputs and can be omitted from the base model.

Reactive transport simulations imply computationally-demanding calculations in terms of required CPU power and memory space. Computational resources depend on the number of degrees of freedom (DOF) of the simulation. The computational grid used for flow and solute transport calculations, as well as the number of chemical elements (total concentrations) determine the number of DOF. Furthermore, the larger the number of variables to be outputted from the simulation, the larger the number of DOF<sup>1</sup>.

The following sections focus on the reduction of the total DOF by reducing the dimensionality of the geometry or the chemical system. A separate section is devoted to the discussion of sensitivity analysis techniques which can be valuable tools for factor fixing.

#### 3.1.2.1 Dimensional reduction of flow and reactive transport

A reduction of the spatial dimensionality is the most obvious application of this MA technique. Three – dimensional representations might be redundant and often a 1 or 2D model will suffice. This simplification must then be justified by the fact that physical properties can be assumed uniform and homogeneous in the remaining spatial dimensions. However, it must be noted that hardly ever three-dimensional reactive transport simulations are performed due to computational limitations, by default most calculations are restricted to one or two dimensions before even attempting a calculation. This implies the assumption that all properties are uniform in all other directions, which is not always completely defensible but would produce acceptable results in most scenarios.

## CASE STUDY REACTIVE TRANSPORT MODELLING OF CONCRETE DEGRADATION

A recent study [23] simulated concrete degradation and leaching in the context of a geological disposal facility of LILW metallic waste. The vault for the metallic waste (BHK) is planned to be backfilled with concrete, which acts as a barrier against

---

<sup>1</sup> The number of DOF of a transient 3D reactive transport problem is obtained as:  
 $\text{No.DOF} = \text{No.mesh nodes} \times \text{discretisation order factor} \times (\text{No.chemical elements} + \text{No.coupled variables}) \times 4$

groundwater flow and contributes to a low diffusion rate and high sorption of many radionuclides.

The authors gradually increased the dimensionality (and scale) of the model by going from 1D, then a 2D cross-section of a BHK vault, a 3D model of a concrete compartment in the BHK vault and finally a model of the entire vault. One important difference comparing model setup for 3D and 2D geometries concerns the treatment of the Darcy velocities across the repository. In the 2D models, an average value was used, which was obtained by averaging the velocities from a 3D hydrogeological model. The 2D simulation case considered a constant inlet flow boundary condition for groundwater flow. In the 3D case, the pressure field from the hydrogeological model was directly imposed as a boundary condition for the compartment and the vault-scale models.

As a result, velocities are higher than the value used in the 2D simulations and the velocity field shows a heterogeneous distribution across the concrete backfill.

In terms of overall portlandite dissolution over time in the modelled domain (divided into concrete and waste domains), it is observed how portlandite is gradually dissolved and leached out of the system, with a higher rate in the 3D simulation case. This is due to the higher local velocities, especially near the concrete outer boundary (see *Figure 3-3*). The CPU times were respectively 17 times and 104 times higher than the time needed to solve the corresponding 2D simulation case for 50 000 (compartment model) and 8 500 years (vault model).

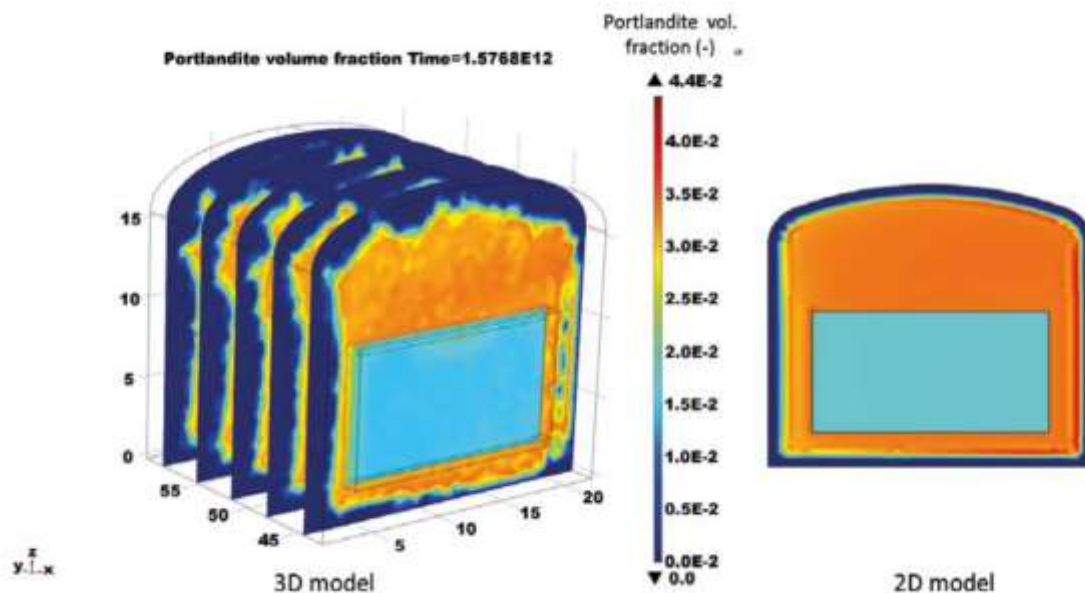


*Figure 3-3: Portlandite volume fraction (–) after 50 000 years: comparison of the results of the 3D compartment-scale model (left) and the 2D simulation (right), taken from [23].*

CASE STUDY: SUB-GRID SCALE REFINEMENT

A more advanced application of this MA technique is to apply this reduction of dimensionality to a small, but highly influential part of the computational domain.

This would be beneficial in the case when the assessment requires simulation of flow and transport processes occurring at large scale in the natural barrier system of the host rock, and simulation of processes occurring at small scales (such as buffer/backfill saturation and waste package degradation) in the engineered barrier system of the repository. Though it is possible to discretize specific portions of the model domain at finer resolution, the disparity in scales of interest presents a challenge in maintaining a computationally manageable problem size. In [24], the authors explored the possibility of using finely-discretized one-dimensional (1D) continua embedded in a three-dimensional (3D) model domain to achieve subgrid-scale refinement in and around each waste package in a simulation of a generic repository. This approach has the potential to save millions of grid cells (and a proportionately larger number of unknowns) in comparison to finely discretizing the 3D model domain in the region of the repository. Because the 1D continua connect to the larger 3D grid at the outermost shell only, their use is appropriate when radial transport (of gas, liquid, heat, and solutes) inward and outward from the waste package is expected to dominate within each volume represented by a 1D continuum, as is the case within a disposal drift filled with low permeability backfill. This idea is related to the fracture-matrix modelling techniques like MINC or DCDM as described in section 3.1.1.1, which are basically virtual, extra dimensions. The commercial finite element code COMSOL Multiphysics has an inherent capability for adding extra dimensions [25]. Extra dimensions can be used to extend a standard geometry with additional spatial dimensions. Using extra dimensions it is possible, in principle, to solve PDEs in any number of independent variables, beyond 3D and time.

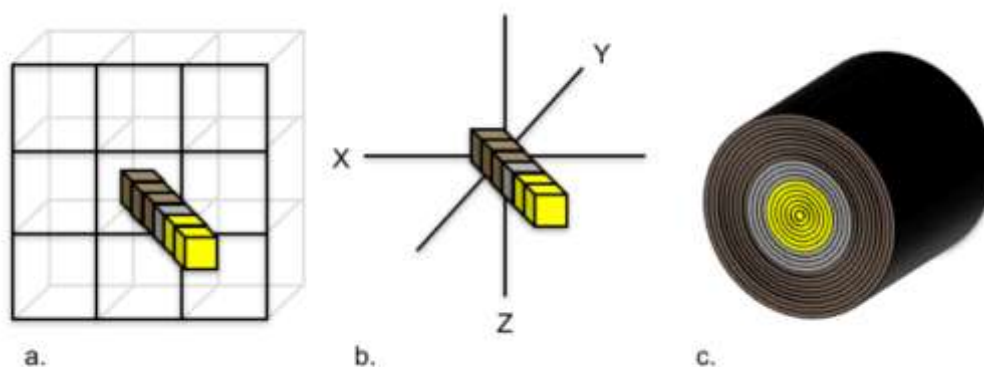


Figure 3-4: a) A 1D continuum is embedded in a 3D grid that occupies the X, Y, and Z dimensions. b) The 1D continuum occupies a virtual 4th dimension; one end of the 1D continuum coincides in space with a cell center in the 3D grid. c) Cell volumes and connection areas within the 1D continuum represent concentric shells of a cylindrical volume occupying the volume of the connected 3D cell, taken from [24].

A similar approach is used in [26], where a radial near-field model following the trajectory of a generic horizontal drillhole is embedded in the Cartesian grid of the geosphere model using the iTOUGH2 software (Figure 3-5).

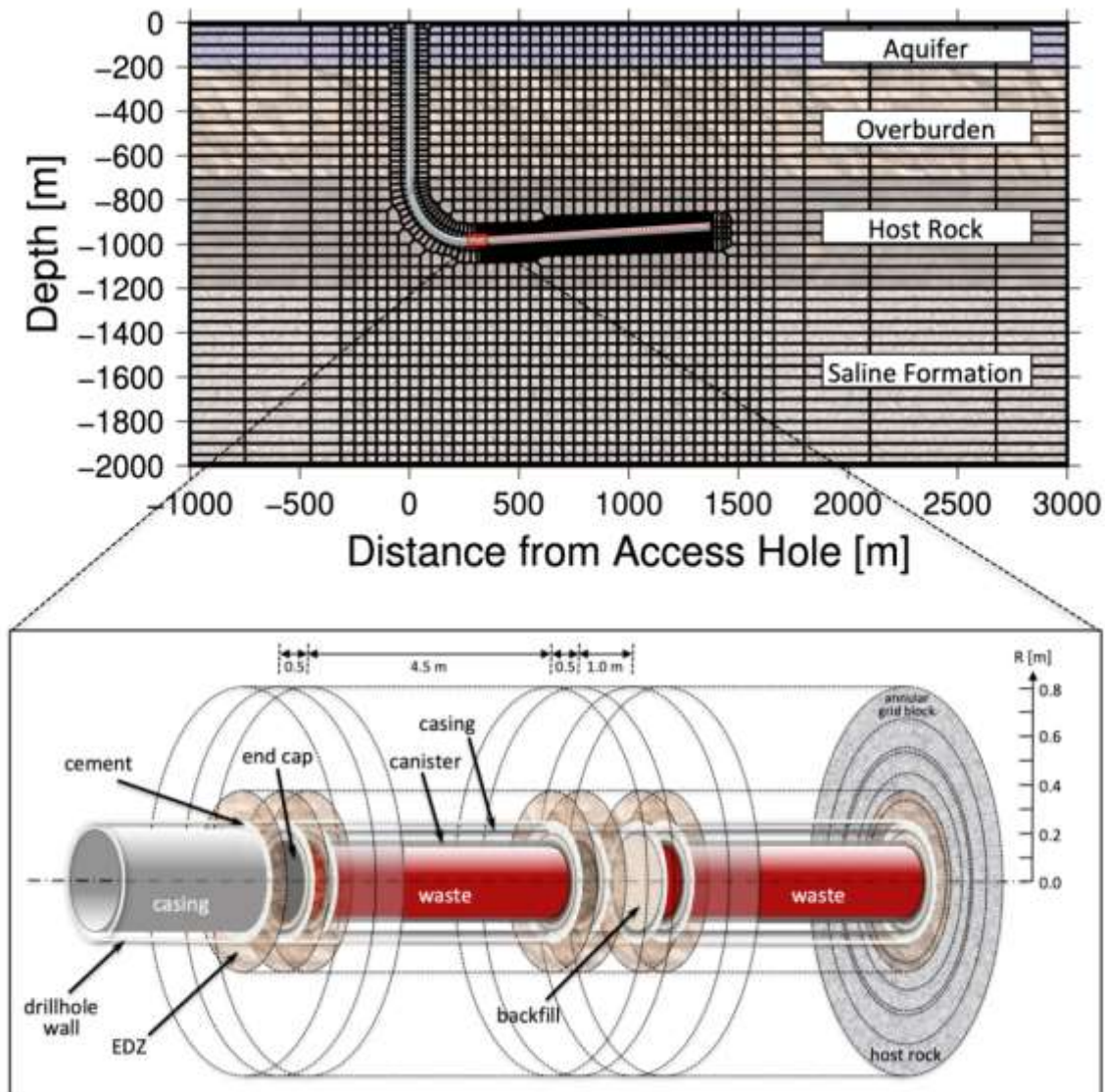


Figure 3-5: Computational grid: (top) excerpt of two-dimensional, vertical cross-section of the three-dimensional Voronoi grid of the geosphere; (bottom) excerpt of radial-axial grid of near-field; the radial-axial grid of the near-field model follows the trajectory of the drillhole and is embedded in the Cartesian grid of the geosphere model. All computational cells of the near-field model are ring-shaped annular grid blocks. The radial discretization is shown on the rightmost cross section; interface radii conform to material interfaces between waste, canister, backfill, casing, cement, excavation disturbed zone (EDZ), and host rock. Outside the maximum radius shown here, the host rock is discretized using logarithmically increasing interface spacings up to a radius of 10 m, at which point the radial-axial grid is connected to the three-dimensional Voronoi grid of the geosphere, taken from [26].

### 3.1.2.2 Dimensional reduction of the chemical system

Reducing the complexity of the chemical system results quickly in a significant reduction of the #DOFs and improves the computational efficiency of the calculation. Sensitivity analysis and/or machine learning techniques can assist in making objective decisions when doing so.

#### CASE STUDY: EFFECT OF SIMPLIFIED CEMENT CHEMISTRY

The effect of the level of sophistication of the chemical system on the degree of concrete degradation has been also studied in [23]. The goal has been to optimize the computation time without compromising the main chemical processes leading to degradation and porosity increase.

The full chemical system refers to the concrete degradation model proposed by [27] for modelling the evolution of concrete in the Final Repository for Short-lived Radioactive Waste(SFR) repository. In the simplified chemistry setup, the amount of included primary and secondary species is reduced. C-S-H jennite-like and C-S-H tobermorite-like are the only C-S-H gels that can precipitate or dissolve following portlandite dissolution. Calcite, ettringite, and gypsum are the other secondary minerals that are considered in the simplified chemical domain compositions.

In terms of pH and porosity evolution, the simple setup provides accurate results. Only slight deviations between the two cases can be observed, with very small differences along the entire profile.

### 3.1.2.3 Dimensional reduction of coupled phenomena

When the amount of considered feedback mechanisms is reduced, this also reduces the dimensionality of the problem, and can lead to drastic performance improvements. However, it might not always be justified. An example is given in the case study below.

#### CASE STUDY: RELEVANCE OF THE POROSITY FEEDBACK EFFECT ON THE GEOCHEMICAL EVOLUTION OF A HLW REPOSITORY IN CLAY [28]

The changes in porosity caused by mineral dissolution/precipitation and the associated changes in flow, transport and chemical parameters of porous and fractured media are relevant for the geochemical time evolution of natural and engineered underground systems. The realistic representation of natural systems requires modelling tools accounting for the changes in porosity. Águila and coworkers investigated the significance of the dynamic update of the flow, transport and chemical parameters in reactive transport models with mineral dissolution/precipitation. The water flow, heat transfer and multicomponent reactive solute transport code, CORE<sup>2D</sup>V5, was extended to take into account the changes in porosity provoked by mineral dissolution/precipitation and their effect on flow, solute transport and chemical

parameters. The improvements implemented in the code were verified against analytical solutions and the numerical solutions computed with other reactive transport codes with similar capabilities for isothermal mineral dissolution/precipitation test cases. Model results computed with CORE<sup>2DV5</sup> agree with the analytical and numerical solutions for several isothermal test cases with porosity feedback. Model results show that neglecting the porosity feedback leads to large differences between different model results. The porosity feedback effect (PFE) is especially relevant in long-term problems with mineral dissolution/precipitation leading to strong changes in porosity. The relevance of PFE was analysed with a non-isothermal geochemically-reactive transport model of the long-term ( $4 \cdot 10^4$  years) interactions of compacted bentonite with corrosion products and concrete in a high-level radioactive waste repository in clay. The model predicts pore clogging in the concrete and at the concrete-clay interface. The major differences of the porosity computed with and without the PFE occur in the concrete and at the concrete-clay and canister-bentonite interfaces. The thickness of pore clogging in the concrete and in the concrete-clay interface computed with the PFE is smaller than that computed without the PFE. The zones affected by clogging in the concrete at  $t = 4 \cdot 10^4$  years computed with and without the PFE are 1 and 4 cm thick, respectively. The thickness of clay affected by clogging near the concrete interface is 0.8 cm with the PFE while it is 1.7 cm without the PFE. In addition, there are zones affected by pore clogging in the concrete near the clay interface and at the canister-bentonite interface in the model without the PFE. However, porosity clogging does not occur in these areas in the model with the PFE. On the other hand, there are significant differences in the mineral volume fractions computed with and without the PFE after  $4 \cdot 10^4$  years. The model with porosity the PFE calculates less magnetite precipitation than the model without the PFE at the bentonite-canister interface. The patterns of portlandite dissolution in the concrete computed with and without porosity the PFE show differences. The model results computed with the PFE show less precipitation of gypsum, brucite, sepiolite and analcime and more precipitation of calcite at the concrete-clay interface than those calculated without the PFE. The largest differences in the computed pH after  $4 \cdot 10^4$  years occur at both sides of the concrete-clay interface. They concluded that reactive transport models presented here demonstrated that the dynamic update of flow and transport parameters is especially relevant in long-term problems with mineral dissolution/precipitation reactions leading to strong changes in porosity.

### 3.1.2.4 Sensitivity analysis

There are a few general textbooks dealing with sensitivity analysis (SA) [5], [29]–[32]. Sensitivity analysis and uncertainty analysis are often performed concurrently, they have different purposes. Uncertainty analysis involves the propagation of uncertainties on input parameters to the resulting uncertainty of output quantities. This is frequently done with (pseudo-)random sampling. In sensitivity analysis, the goal is to identify the most influential parameters affecting the results. Determining the strength of the relation between a given uncertain input and the output is the job of sensitivity analysis. This is often done using the same samples generated as part of an uncertainty analysis process. Sensitivity analysis can be a powerful tool to assist in the simplification or abstraction of highly parametrised models, as explained later.

For sensitivity methods, one can roughly distinguish between [31]:

- **Local analysis:** The model output is analysed locally with respect to a reference/working point, to identify the steepest gradient as most important direction of change, apportioning local change to the different inputs. In these local sensitivity measures the effect of the input factor is observed while assuming all other factors fixed. These methods fall in the class of the one-factor-at-a-time (OAT) methods.
- **Screening methods:** The model is analysed with predefined bounds on the input parameters, to identify (screen out) input parameters with little influence, apportioning global change to the different inputs. The Morris elementary effects quantify the mean absolute value of the changes in the model output,  $Y$ , due to the perturbations in the model input parameters,  $\{x\}_i$ . Morris effects are useful to identify the relevant and irrelevant input parameters. The Morris method provides global sensitivity measures because the mean changes in  $Y$  are computed at a large number of parameter combinations evenly distributed in the parameter domain.
- **Global methods:** The model output is analysed with a known distribution of the inputs, apportioning the uncertainty in the output to the different inputs.

### 3.1.2.5 Global sensitivity analysis

Global methods can be used in different sensitivity analysis settings [5]:

- **Factor prioritization (FP):** Finding the most important input parameters.
- **Factor fixing (FF):** Finding the least important input parameters.
- **Trend identification (TI):** Identify monotonicity or convexity properties of the model.
- **Structure discovery (SD):** Uncover additivity, linearity, interactions.
- **Regionalized sensitivity (RS):** Finding active regions of input parameters.

Most chemical models in reactive transport are of a rather non-linear nature. Non-monotonic and non-additive features are also common. For these models, local OAT methods should be avoided as they do not identify interactions among factors and are

extremely poor at exploring multi-dimensional factors spaces. To this purpose, global methods should be used. An important example of global methods are the variance decomposition methods.

Variance-based indices apportion the output variance to the contributions from various input parameters. Under input independence, each square integrable function can be decomposed into orthogonal functions (with respect to the input probability),

$$\begin{aligned} g(x) &= g_0 + \sum_{i=1}^d g_i(x_i) + \sum_{j>i} g_{i,j}(x_i, x_j) + \sum_{k>j} g_{i,j,k}(x_i, x_j, x_k) + \dots + g_{1,2,\dots,d}(x) \\ &= g_0 + \sum_{i=1}^d \sum_{|\alpha|=i} g_\alpha(x_\alpha) \end{aligned}$$

such that the output variance can be decomposed into  $\mathbb{V}[Y] = \sigma_Y^2 = \sum_{i=1}^d \sum_{|\alpha|=i} \sigma_\alpha^2$  where the contribution of input group  $\alpha$  is defined recursively via  $\int g_\alpha(x_\alpha)^2 f_\alpha(x_\alpha) dx_\alpha = \sum_{\beta \subset \alpha} \sigma_\beta^2$ . It also holds that  $\mathbb{V}[\mathbb{E}[Y|X_\alpha]] = \int g_\alpha(x_\alpha)^2 f_\alpha(x_\alpha) dx_\alpha$ , the conditional output variance given the input group of interest is obtained by integration from this functional decomposition. This decomposition is called functional analysis of variance (ANOVA).

The relative contribution to the output variance is then the variance-based Sobol' effect for the index group  $\alpha$ ,  $S_\alpha = \frac{\sigma_\alpha^2}{\sigma_Y^2}$ . The first order effect is given by  $S_i = S_{\{i\}}$  and the total effect is given by  $T_i = \sum_{i \in \alpha} S_\alpha$ .

Estimation of the variance contribution via the functional ANOVA decomposition is very cumbersome. Sobol [33] came up with a special design that allows a more efficient estimation of first and total effects. The original idea was later improved by several researchers (see e.g. [34], [35]).

The total effects calculated using Sobol' method for variance-based sensitivity effects are the current gold standard in a factor fixing setting, whereas the first order effects yield information on factor prioritization and additivity. The drawback of variance-based methods is the relative large amount of model realizations they require, often generated according to a specific sampling scheme. If the objective of the SA is to fix non-influential factors and model is expensive to run, screening methods (e.g. Method of Morris) become attractive. Processes with parameters that have low total effects (or sensitivity indices) are non-influential and can be removed from the model in order to simplify future analyses. As such, global sensitivity methods can have an important contribution to the process of model abstraction. That is, if the computational cost of the sensitivity analysis does not outweigh the potential benefits of the simplification.

Global sensitivity and uncertainty quantification methods have been widely used in performance assessment studies to quantify the prediction uncertainties caused by uncertainties in flow and transport parameters ([36]–[38]). A few studies have analysed

the uncertainties in using reactive transport models. The authors of [39] developed a preliminary uncertainty analysis tool for performance assessment calculations considering uncertainties in the groundwater concentrations of Na, Ca, HCO<sub>3</sub> and Cl. Monte Carlo methods were applied in ([40], [41]) to pure geochemical code calculations for investigating (a) the significance of uncertainties in predicted pH values for a simple buffer solution and for calcite saturation indices, and (b) the effects of database parameter uncertainty on uranium(IV) equilibrium calculations (i.e. uranium(IV) speciation), respectively. [42] presented a model to estimate the uncertainty associated with the amounts of CO<sub>2</sub> generated by carbonate-clays reactions in subsurface systems. Recently, [43] presented a comprehensive uncertainty and sensitivity analysis of Cs sorption reactive transport modelling with 3 cation exchange sites in the near field of a deep geological repository for nuclear waste based on the Morris and Sobol methods. The uncertainties were analysed in: 1) Cation exchange selectivity coefficients and 2) Clay pore water cation concentrations. They were able to identify the most important uncertain parameters affecting the transport of cesium and the combination of parameters values leading to the maximum cesium concentrations at a specified location using classification trees. Finally, they proposed a cesium isotherm and a K<sub>d</sub> uncertainty range based on a large number of numerical simulations.

Recently, in [44], [45] the use of global sensitivity methods for radioactive decay chains which combine the values of the output variable and its derivatives is reported. The derivatives were calculated with the adjoint state method.

#### CASE STUDY: SENSITIVITY ANALYSIS FOR CHEMICAL MODELS

Saltelli et al. ([46], [47]) focus on the most promising modern approaches to SA for chemical models, especially the variance-based global sensitivity analysis methods. The authors illustrate the usefulness of SA using a few worked examples related to complex chemical reaction schemes and discuss the performances of different kinds of local, global, meta-modelling or screening-based measures.

CASE STUDY: SENSITIVITY ANALYSIS TO GUIDE SIMPLIFICATION OF GEOCHEMICAL SYSTEMS

C. Holle et al. [48] applied unsupervised machine learning (ML) tools to inputs and outputs of a reactive transport model for CO<sub>2</sub> sequestration [49] to identify and extract only the dominant geochemical species in order to reduce execution times. Matrix factorization was used to discover hidden features (in this case dominant geochemical species) in a database. They applied Non-negative matrix factorization combined with customized k-means clustering (NMFk) to data from reactive-transport simulations to estimate the minimum number of species, minerals, and input variables required to sufficiently describe a reactive-transport system. They found that about three species, six minerals, and four variables were sufficient to describe the system.

3.1.2.6 Connection to WP DONUT Sensitivity analysis work by ENRESA/UDC

This section describes the work of ENRESA/UDC in DONUT regarding local and global sensitivity methods, meta-models and benchmarking of reactive transport models.

ENRESA(UDC) contributes to DONUT Task 4 with innovative adjoint-state methods and global sensitivity and uncertainty analyses for reactive transport models.

The adjoint state (AS) equations for solute transport have been derived for the continuous and discrete versions of the original problem. Both the continuous and discrete adjoint state equations are linear. The adjoint state of the transient solute concentration,  $\tau$ , is solved by proceeding backwards in time, and starting at the final conditions where  $\tau = 0$ . The steady adjoint state,  $\tau_0$ , is solved afterwards.

Although the discrete and continuous adjoint state methods lead to different algebraic equations, their solutions are consistent because both methods reflect different ways of discretizing the same partial differential equations. The continuous method is versatile because it allows using a numerical method and a discretization scheme for the adjoint states independent of those of the forward problem. The discrete AS method, on the other hand, must be developed specifically for the code of the forward problem. Therefore, it is an intrusive method. The discrete AS method offers the advantage of ensuring a numerical accuracy of adjoint state similar to that of the forward problem.

ENRESA/UDC is using global sensitivity methods (Sobol, Morris and VARS) for the reactive transport model of the long-term geochemical evolution of a HLW repository in granite (Task 4 of ACED).

ENRESA/UDC participates also in the following reactive transport benchmark test cases of DONUT Task 5:

- 1) Geochemical Machine-learning (ML) benchmark. This benchmark is designed to test a variety of ML techniques relevant to geochemistry and reactive transport, aiming at generating high quality data for training/validation of

existing/new methodologies and at providing basic guidelines about the benefits and drawbacks of using ML techniques.

- 2) Nonisothermal multiphase flow and reactive transport benchmark. The proposed benchmark tests cases are related to:
  - a. The nonisothermal post-closure unsaturated stage of the engineered barrier of a HLW repository, in which strong temperature gradients are present with water evaporation near the canister;
  - b. The formation of a gas phase in the engineered barrier due to hydrogen release from carbon-steel canister corrosion. The main features of the non-isothermal multiphase flow and reactive transport benchmark include the thermal gradient caused by the heat released from the waste, the multiphase flow of air, vapour and liquid water, bentonite swelling, canister corrosion, concrete degradation and geochemical reactions involving aqueous, exchanged, sorbed and mineral species.

### 3.1.3 Scale change

#### 3.1.3.1 Upscaling

Flow, transport and reactive processes can be treated at different scales: (i) the molecular scale, (ii) microscopic scale treating the fluid as a continuum, (iii) the macroscopic local scale treating the porous medium as a continuum, and (iv) the macroscopic formation scale treating the field-scale as a continuum. Processes at a subsequently larger scale can be obtained by averaging the smaller scale and defining transfer coefficients, or by defining equations at a given scale (e.g., Darcy's law for water flow at the porous medium continuum).

Macroscopically observed chemical and transport phenomena are strongly related to the processes that take place at the pore and the atomistic scale. Within porous media, the transport of solutes is affected by the interaction with the mineral surfaces, the pore connectivity and the pore geometry. The kinetics of (mineral) dissolution and precipitation are controlled by the supply of reactants to, and the removal of reaction products from, the mineral surface and the intrinsic surface reactivity. The macroscopically measured reaction kinetics is thus an interplay of mass transport and surface reactivity [50].

There are numerous upscaling techniques: volume averaging [51], homogenization [52], renormalization [53], [54], ensemble averaging [55], and continuous-time random walk [56].

CASE STUDY UPSCALING OF FLOW/DIFFUSION PROPERTIES FROM PORE SCALE TO CONTINUUM SCALE [57]

In geochemically reacting environments, the mineral dissolution and precipitation alters the structural and transport properties of the media of interest. The chemical and structural heterogeneities of the porous media affect the temporal evolution of the permeability with respect to porosity. Such correlations follow a nonlinear trend, which is difficult to estimate a priori and without knowledge of the microstructure itself, especially under the presence of strong chemical gradients. However, these inputs are required for macroscopic field- scale models.

The authors performed pore-level simulations which provide the basic understanding of the underlying mechanisms (preferential flow, mineral precipitation and dissolution,...) which dictate the structural evolution of the porous medium. The authors then discussed three different possible upscaling strategies.

The permeability-porosity correlations that are modelled in a macroscopic code are replaced with more precise and case-specific correlations. First, the result can be transmitted in the form of power law or Kozeny-Carman type of function. Second, tabulated values can be provided instead of a power law, such that during the macroscopic simulations, specific values can be calculated, after interpolating between successive points. Third, the macroscopic code could call on demand the pore-level solver, to deliver the prediction of evolution in a fully coupled multiscale manner.

CASE STUDY: UPSCALING OF GLASS DISSOLUTION IN A FRACTURED VITRIFIED NUCLEAR WASTE CANISTER

In this study [58] efforts were made to bridge the gap between the reservoir-scale flow and transport simulations and the micron-scale modelling of the glass-water interfacial processes by providing quantitative evaluation of the aqueous alteration of glass at the block scale. This resulted in the calculation of the equivalent diffusive, hydraulic, and alteration kinetics properties. Prior to performing reactive transport modelling at the scale of the glass canister, several upscaling techniques were first applied to a synthetic fracture network system with ends to compare the results of the borosilicate glass alteration with the discrete fracture modelling and the equivalent porous medium approach (*Figure 3-6*). The evolution of the altered glass obtained from reactive transport modelling applied to several realizations of the equivalent fracture network tessellation was then compared to the experimental data of the aqueous alteration test of a nonradioactive full-scale SON68 glass canister. The proposed model agrees well with the experimental data.

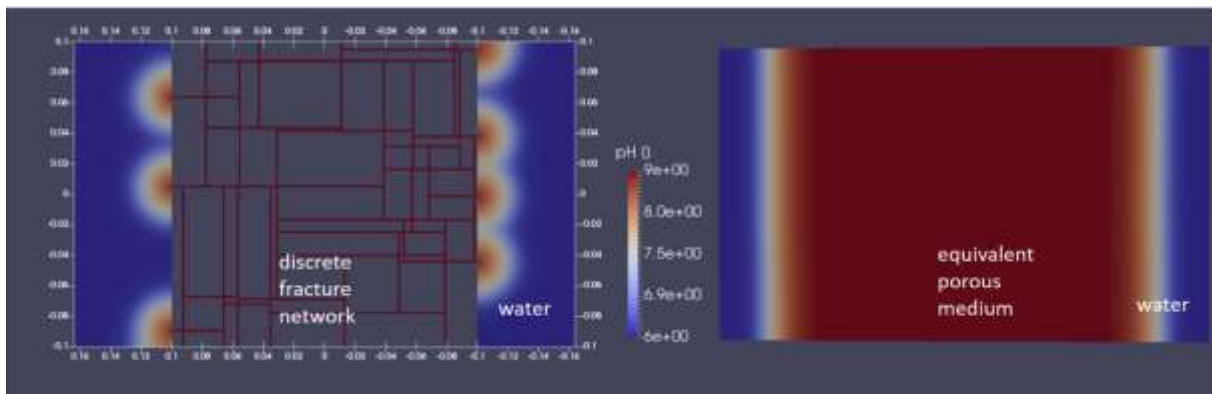


Figure 3-6: Physical representation of the system comprising two reservoirs and the synthetic fracture network in the framework of a) the discrete model and b) the equivalent porous media model, taken from [58]

### 3.1.3.2 Aggregation

Unlike in upscaling, no relationship is assumed between model parameters at the fine and at the coarse scales. Parameters of the coarse-scale model are deemed to be lumped. Aggregation can be also done without the change in the model equations by combining several materials. When applied to flow and transport in vadose zone, one common application is to replace a heterogeneous soil profile with an equivalent homogenous profile while retaining the Richards equation as a flow model.

### 3.1.4 Reduced numerical accuracy

In this class of strategies, the lower-fidelity models are fundamentally the same as the original models but with reduced numerical accuracy. A lower-fidelity model can be a variation of the original model but with larger (coarser) spatial/temporal grid size.

Discretization errors are defined as the difference between the exact solution of the conservation equations and the exact solution of the algebraic system of equations obtained by discretizing these equations [59]. Obviously, discretization errors increase with increasing grid spacing.

There exist two categories of estimators for this discretisation error. The first category of discretization error estimators is based on estimates of the exact solution to the differential equation which are higher-order accurate than the underlying numerical solution(s) and include approaches such as Richardson extrapolation, order refinement, and recovery methods from finite elements. The second category of error estimators is based on the residual (i.e., the truncation error) such as discretization error transport equations, finite element residual methods, and adjoint method extensions.

The Richardson extrapolation technique is the most well-known and used as it can be applied as a post-processing step to the solution from any discretization method (e.g., finite different, finite volume, and finite element). Regardless of the approach chosen,

the discretization error estimates are only reliable when the numerical solutions are in the asymptotic range, which requires at least three systematically refined meshes to be demonstrated. For complex numerical computations involving coupled, nonlinear, multidimensional, multi-physics equations, it is unlikely that the asymptotic range will be achieved. The most common situation in scientific computing is when the discretization error estimate has been computed, but the confidence in that estimate is either 1) low because the asymptotic range has not been achieved or 2) unknown because three discrete solutions are not available. In these cases, the discretization error is more appropriately characterized as an epistemic uncertainty due to the lack of knowledge of the true value of the error. Roache's Grid Convergence Index effectively converts the error estimate from Richardson extrapolation into an uncertainty by providing error bands. For more details on methods for estimating discretization error in scientific computing, see [60].

Finite element models with lower discretisation order can also be a low-fidelity model of an original model. Whenever applicable, lower-fidelity models can be essentially the same as the original model but with less strict numerical convergence tolerances.

It must be noted that a coarser mesh and time-stepping leads to reduced accuracy but also reduced robustness. A reduced discretisation order (linear, quadratic, ... elements) leads to reduced accuracy but sometimes an increased numerical stability or robustness.

An example of the influence on reduced meshing density on numerical accuracy is given in appendix A and B, an extra example on the reduction of dimensionality is given in Appendix C.

### **3.2 Response surface surrogate modelling or Meta-modelling**

This is a group of abstraction methods that use results of multiple simulation runs to extract the information helpful to simplify a complex model. The metamodel creates a computationally efficient model intended to mimic the behaviour of the complex model, that is, to reproduce the object model's input-output relationships [61]. A common way to develop a metamodel is to generate "data" from a number of large-model runs and then to use the statistical methods to relate the model input to the model output without attempting to understand the model's internal working.

The statistical emulator typically incurs a negligible computational cost compared to that of the original model such that the available computational resources can be fully dedicated to the emulator construction. Of course, the success of this approach will largely depend on the surrogate model accuracy, that is, the extent of the bias between surrogate and original model predictions. For a given computational budget, this bias will in turn be controlled by the degree of nonlinearity and parameter dimensionality of the original model.

There is a wide range of statistical techniques available in the statistics/machine learning and hydrology literatures for emulating the behaviour of computer models

(see, e.g, review papers of [2], [62], [63] , all presenting some advantages and drawbacks).

Meta-models can be used to emulate the full reactive transport model (§3.2.1), to (partially) replace the solver of the geochemical step in reactive transport codes (§3.2.2) and to replace computationally expensive process models (§3.2.3).

Please note that throughout the remainder of the document, terms like meta-model, surrogate model, emulator,... are used alongside each other. Basically, they all mean the same thing.

### 3.2.1 Meta-modelling on full reactive transport models

In [64], the authors compare machine learning techniques for emulating the full reactive transport models (that is flow, transport and geochemical reactions), for a sensitivity analysis and uncertainty propagation, used for migration modelling of uranium U(VI) from radionuclide contaminated sediments. Among other, they compare the efficiency of neural networks and highlight advantages and disadvantages of different simulation strategies. A highly detailed theoretical background about neural networks is presented in [65].

### 3.2.2 Meta-models used to replace the geochemical solver

For realistic system descriptions, the chemical reactions and speciation calculations are the parts of the algorithms that consume most of the computational time, when compared to the time needed for the mass transport calculations. Lately, there has been a number of efforts to accelerate only the geochemical calculations in coupled reactive transport models by using machine learning techniques to replace the geochemical solver [50], [63], [66]–[71].

Jatnieks et al. [66] propose to replace the geochemical model by a data-driven surrogate model. They compare 32 statistical and machine learning methods on a 1D case study corresponding to the injection of a reactive solution leading to the dissolution of calcite and the precipitation of dolomite. Their results show a good agreement with the simulation results and highlight that accuracy highly depends on the training sample. The authors identified the neural-network based techniques as the most promising ones. In [68], a machine learning approach is proposed (look-up table) to calculate equilibrium states in reactive transport simulations where the learning is carried out during the actual simulation without an initial training phase. This approach leads to an impressive speed-up factor in the range of 60–125.

In [72], both a fully data-driven approach and a geochemical knowledge-informed surrogate model approach are described and tested. The authors found that decision-tree based methods such as Random Forest and their recent gradient boosting evolutions appear the most flexible and fit for purposes. The surrogate models were trained during the initial stages of the reactive transport calculation. Further on, when the output of the trained surrogate model resulted in a too large mass-imbalance, the result is discarded and the geochemical solver is called instead. This prohibits a gradual build-up of mass balance errors during consecutive iterations which can lead to unphysical results.

Since metamodels may not always yield sufficiently mass-conservative results, the metamodels can be used as predictors of the initial guess for the geochemical solvers. If the metamodel provides accurate estimates, this strategy may lead to a large decrease in number of iterations of the geochemical solver.

### CASE STUDY: ANN GEOCHEMICAL SOLVER FOR CALCITE PRECIPITATION

Guérillot and Bruyelle [69] presented a 3D case study concerning CO<sub>2</sub> storage in a geological formation. In order to simulate these reactive transport processes, geochemical equations (equilibrium and kinetics equations) were coupled with multiphase flow and transport in porous media in order to represent calcite precipitation/dissolution phenomena using the framework of a sequential non-iterative SNIA reactive transport code. The authors used artificial neural networks (ANN), which are trained during runtime, to calculate the geochemical equilibrium instead of the actual geochemical solver to speed up the simulations.

When a reasonably sized training set was used, the authors showed the high capability of the ANN to reproduce the geochemistry calculations. The speed-up factor, ignoring the initial training phase, was equal to 45.

It must be noted that the resolution of the geochemical system by the meta-model, cannot be fully mass-conservative. The error generated at each time-step grows with time. The absolute increase of error highly depends on the accuracy of the ANN. However, it can be reduced by expanding the learning phase when the input parameter space is covered more efficiently.

When the ANN method is applied to a fully reactive transport 3D calculation (of 3300 cells), the speed-up factor reduces to 14. Most cells of the domain are not exposed to high chemical gradients as they are located far away from the CO<sub>2</sub> injection well. The geochemical solver converges within 1 iteration for those cells and consequently the computational gain is limited to the few cells that are at the evolving reaction front. In general, when less time is taken up by the geochemical step compared to the transport step, less advantage is created by the ANN. The figure below shows the amount of calcite that has been dissolved, under kinetic control, due to the drop in pH caused by the CO<sub>2</sub> injection.

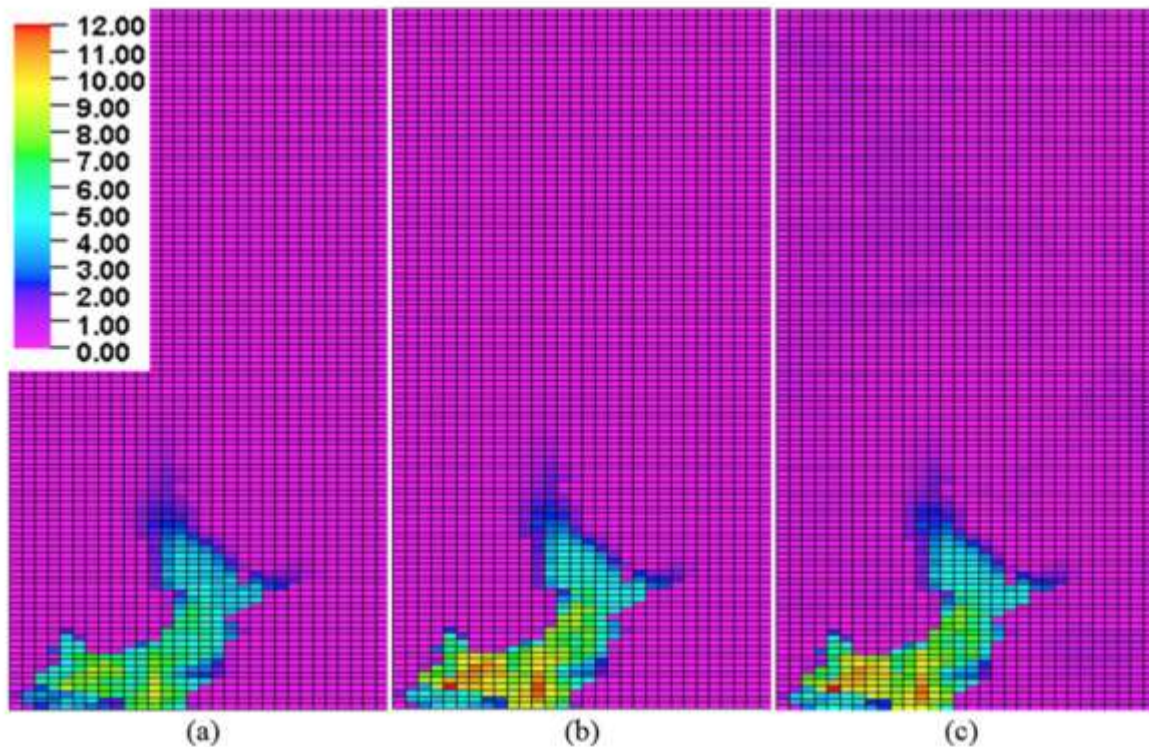


Figure 3-7: Dissolved Calcite (mol). (a) End of CO<sub>2</sub> injection period. (b) End of simulation with geochemical solver. (c) End of simulation with ANN, taken from [69].

### 3.2.3 Meta-models used as replacement of process models

Another promising application of meta-modelling in reactive transport models used in the framework of radioactive waste disposal is to introduce surrogates in order to replace computationally expensive process models.

#### CASE STUDY: SURROGATE MODELS FOR WASTE/FUEL DISSOLUTION PROCESS MODELS

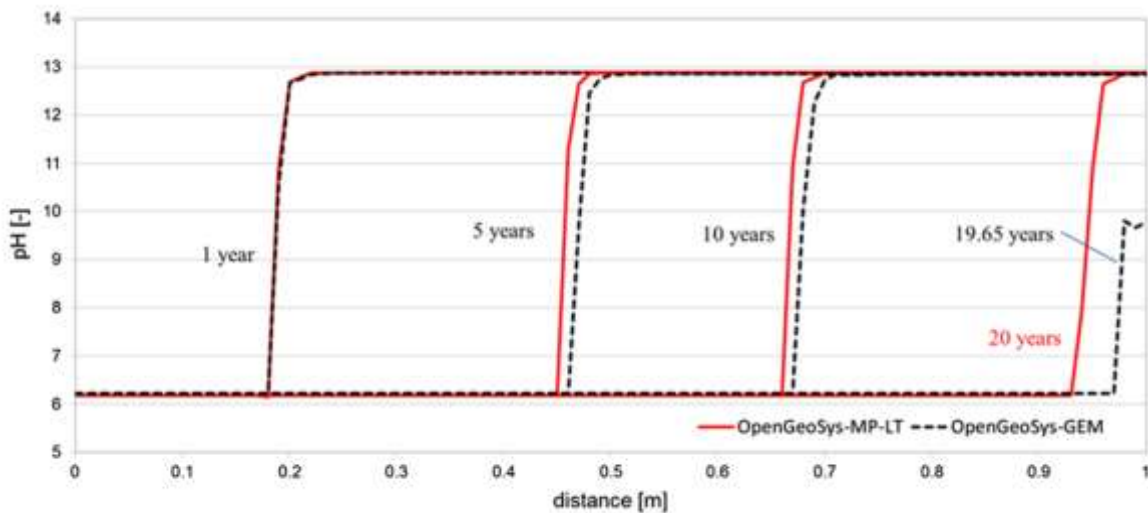
In [24] two types of surrogate models were developed for the spent Fuel Matrix Degradation (FMD) model using artificial neural network (ANN) surrogate and k-Nearest Neighbours regressor (kNNr) techniques. The FMD process model calculates spent fuel degradation rates as a function of radiolysis, alteration layer growth, and diffusion of reactants through the alteration layer. This 1D model outputs UO<sub>2</sub> fuel degradation rates at each timestep based on fuel properties (e.g. burn-up, age,...), temperature and near-field concentrations of H<sub>2</sub>, O<sub>2</sub>, CO<sub>3</sub><sup>2-</sup> and Fe<sup>2+</sup>. The ANN and kNNr FMD surrogates were implemented in PFLOTRAN and then demonstrated in two different repository simulations leading to a significant speed-up.

CASE STUDY: SURROGATE MODEL FOR CARBONATION PROCESS

In these works [73], [74], a new model for fast and efficient simulation of long-term concrete degradation due to alkali-silica reaction (ASR) and carbonation is presented. The model provides an alternative coupling solution of reactive transport and multiphase multi-component flow by approximating the complex chemical reactions into a look-up table, which can further be integrated into a two-phase multi-component transport model via source/sink terms.

A 1-D reactive transport benchmark is proposed by taking into account the two main chemical reactions which drive the concrete degradation: ASR and carbonation caused by transport of CO<sub>2</sub> in a gas phase.

When the numerical model derived from the look-up table approach is compared to a full reactive transport code, it is shown that the look-up table approach and the full reactive transport code produce very similar results for the prediction of degradation of concrete. However, the look-up table approach leads to a considerable reduction in calculation time (factor 14). The comparison of pH and porosity evolution in a benchmark case where CO<sub>2</sub> diffusion dominates, i.e. the progress of carbonation is much faster than the typical time scales for ASR, performed in a 1D setup of a 1 m long concrete domain.



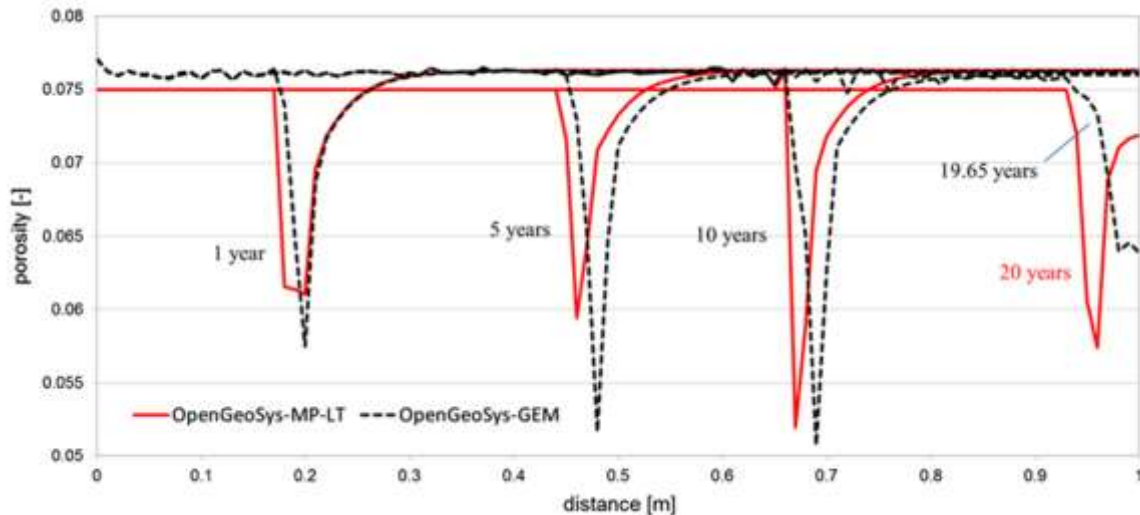


Figure 3-8: Comparison of look-up table approach (MP-LT) and full reactive transport model (GEM): pH and porosity profiles at different times in the carbonation benchmark case. The right side of the simulation domain at 1 m is a closed boundary, taken from [58].

The approach described above bears a certain resemblance to the method described in an earlier publication [75]. The leaching of calcium from the concrete materials is simply described by a single component-model in the aqueous and solid phase. However, The mineral geochemistry is pre-calculated with a multi-component geochemical equilibrium model. Then, univocal relationships between porosity, diffusivity and solid/liquid distribution ratio with liquid Ca-concentration are derived which are read from an interpolated lookup table. Mass exchange between the solid and liquid phase is implemented as a source term in the abstracted model. This allows for an impressive speed-up of the calculations compared to the original multi-component model but still allows a good prediction of degradation fronts both under advective and diffusive conditions.

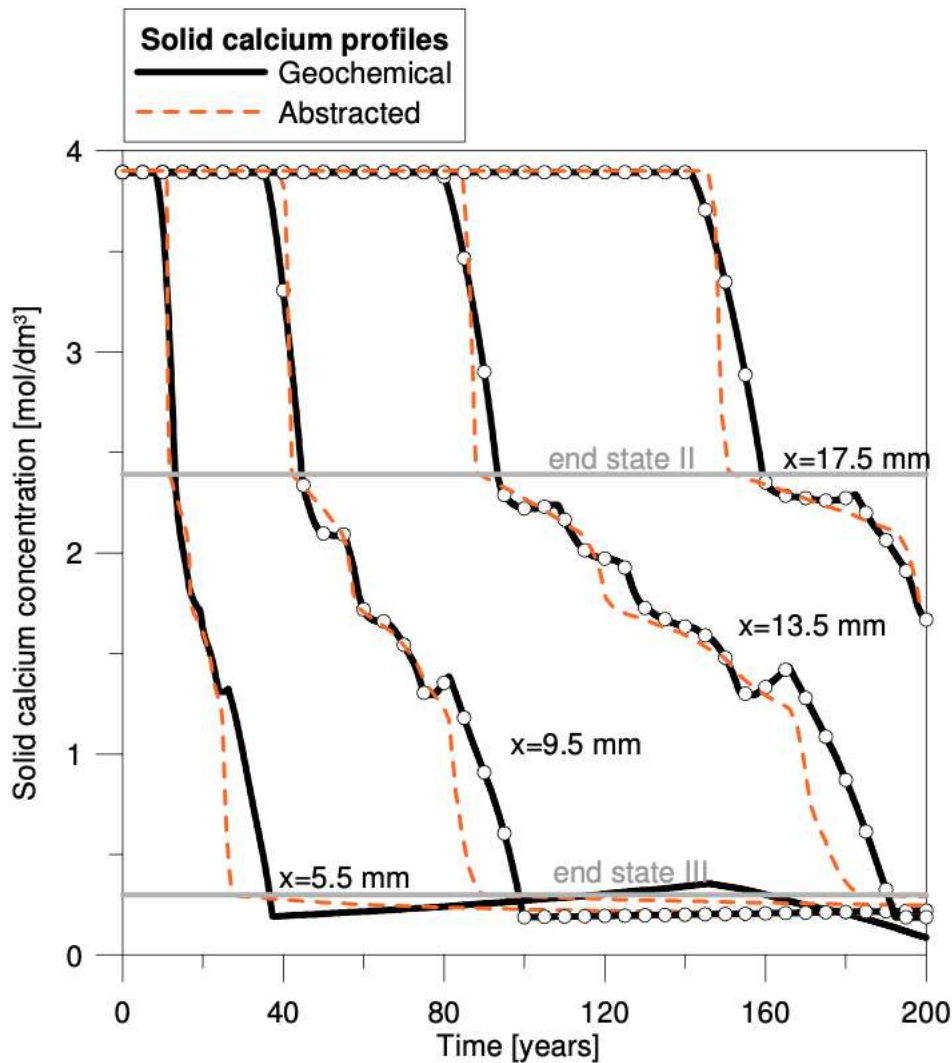


Figure 3-9: Comparison of the solid Ca profiles and the ends of chemical degradation state II and III between the full and abstracted model during diffusive transport conditions, taken from [75].

### 3.2.4 Meta-modelling in DONUT

Methods discussed in section 3.2 will be developed and tested in the framework of (simplified) reactive transport modelling in the WP DONUT – WP ACED concentrates on methods discussed in section 3.1. Several methods (Gaussian processes, kNN, neural networks) are tested for applications in the framework coupled reactive transport with focus on emulating the complete reactive transport model or emulating only the geochemical solver.

Both the geochemical models and the reactive transport models are simpler in DONUT compared with the models described in D2.16. DONUT investigates nevertheless the possibilities and limits of these surrogate techniques; however focussing on a very accurate emulation of the original model. In the framework of model abstraction, this is

## EURAD Deliverable ACED 2.18 – Model abstraction techniques

not always required; the focus is on the output of interest (see definition of model abstraction in §2.1).

DONUT will contain work on two benchmarks in which high quality training sets will be provided for testing different algorithms. One benchmark deals with cement evolution with training sets for different cement models with increasing complexity. The second benchmark deals with U speciation and fate in a clay system (Callovo-Oxfordian clay).

## 4. Discussion

With increasing computational power, reactive transport models often became highly detailed about the processes and resolution they represent. The more processes are understood, the more there is a tendency to incorporate that knowledge into the numerical models.

Reverting to lower-fidelity versions of these detailed models, by using techniques described in section 3.1, might thus seem as a step backwards. It should be carefully thought over if this loss in numerical accuracy or scientific correctness balances the benefits of the decrease in computational burden (for instance an improved quantification of the uncertainties associated with the model). It is therefore important to try to estimate the time and computational gain from the abstraction, as well as human resources available to create the abstracted model and to check and document its validity. For example, if the 1D version of a cement leaching model (discussed in §3.1.2.1) strongly underestimates portlandite leaching due to a poor description of the hydraulics in the vaults compared to a 3D implementation, there is hardly any benefit in running hundreds of simulations with that 1D model to assess the exact uncertainty on the portlandite leaching rate. However, the 1D model might do a better job on predicting pH-evolution in zones which are less affected by water flow and prove sufficiently accurate for that application.

Surrogate modelling approaches offer a big advantage in that they- when constructed correctly- do offer a big gain in speed but do not suffer from a large loss in accuracy or detail. Lately, there has been a number of efforts to accelerate only the geochemical calculations in coupled reactive transport models by using machine learning techniques to replace the geochemical solver. Currently, these surrogate-based techniques have not evolved to the point that they can be readily and fully automatically applied to every reactive transport problem in radioactive waste disposal. At the moment, the method is proven successful on relatively straightforward cases. Research on the topic is continuing and big advances due to improvements in machine learning algorithms and computational resources are expected.

Eventually, it is up to the user to direct the efforts towards improving the computational efficiency of the full model; to invest in a more powerful computational infrastructure; or towards the abstraction or simplification of the model. The choice between these options might depend on the specific research question that the model needs to answer.

## 5. Conclusion

Reactive transport models in the context of radio-active waste disposal tend to become increasingly complex due to advancements in understanding and quantifying of (geo)chemical and transport processes in the engineered barriers and surrounding geological layers.

The complexity of these models is caused by the large number and intricacies of the simulated processes, many interacting species and/or components, differences in scales at which the interactions occur and amount of couplings to simulate. The models can become even more challenging as they have to be applied to long timescales and large spatial scales.

Model abstraction is the field of active research in reactive transport modelling, especially in the context of radioactive waste disposal. Many model abstraction techniques have been developed which are summarized in previous sections. Several case studies have been discussed in order to illustrate the state of the research.

Performing model abstractions will likely result in many benefits. It will foremost improve the understanding of the complex models and (the role of) their essential factors. This again will aid to communicate the modelling results to both a technical and lay public. The reduced computational burden of the model can lead to a more robust uncertainty and sensitivity analysis, which in turn will build the confidence in the model predictions.

However, the model abstraction process should be performed according to a transparent and well-documented procedure which justifies the use of the abstracted model. It must be stressed that those abstracted models are only valid within the ranges they are derived from. Care must be taken when those models are used for extrapolations or when coupled to additional physical models.

Moreover, reverting to lower-fidelity versions of these detailed models, by using techniques described in §3.1, might seem as a step backwards. It should be carefully thought over if this loss in numerical accuracy or scientific correctness balances the benefits that arise from computational speed.

Surrogate modelling (or meta-modelling) approaches offer a big advantage in that they- when constructed correctly- do offer a big gain in speed but do not suffer from a large loss in accuracy or detail. As such, they can be used to accelerate the geochemical calculations in coupled reactive transport models by replacing the

geochemical solver. At the moment, these methods are proven successful on relatively straightforward cases but the research on this topic is continuing and seems promising.

## 6. Appendix A: Reduced numerical accuracy: impact of mesh size

### 6.1 Context

The interacting components in a disposal cell can have steep thermal, chemical and hydraulic gradients. The numerical accuracy of the calculated interaction can depend on the mesh density. There can be different approaches to obtain a sufficient well numerical accuracy e.g. a variable mesh in which the number of mesh elements is larger at the interface between the interacting components or a constant mesh in which the number of mesh elements does not vary as a function of space. For some laboratory experiments, a constant mesh can achieve the same numerical accuracy and can be performed in a similar period in time as a variable mesh. In this section of the report, a constant mesh is used. The transport of water is a key process for the determination of the chemical evolution in a disposal cell. In this section of the report, an example is worked out for which the numerical accuracy was important for the validation of the parameters for the transport of water and gases used in the model.

### 6.2 Example cementitious material

#### 6.2.1 Transport of water

COVRA's waste package mortar is a cementitious material with a sufficient small porosity to allow diffusion of water as the main migration mechanism for the transport of water. The diffusion coefficient is constructed from the Millington-Quirk model. In this model, a porous material is envisaged of solid spheres which interpenetrate each other, separated by spherical pores which also interpenetrate. The solid and pore systems are therefore symmetrical [76]. The value for diffusion of water depends on the saturation degree of the pores. Consequently, the diffusion value for water can vary within a component if the saturation degree is not uniform i.e. so-called non-linear diffusion. The model described in [77] has successfully been used in modelling transport of ions in unsaturated cement-based materials (Samson and Marchand 2007) and can be used at the scale of the waste package scale as well as disposal cell. The model requires the porosity, cementation factor and self-diffusion of water. The porosity can be measured and literature values for the self-diffusion of water are available. Only the cementation factor needs to be validated. For the validation of this parameter, saturated concrete cubical cubes have been exposed to different relative humidity's. The outer surfaces are steep hydraulic gradients. The Millington-Quirk model is implemented in the COMSOL 5.5 module Transport of Diluted Species in Porous Media. There are 9 physics-controlled mesh types included in the software from extremely coarse with a small mesh density till extremely fine with a high mesh density. The numerical accuracy but also the computational time increase with increasing mesh density. Table 1 shows the used mesh densities and required computational time for the calculated results in *Figure 6-1*.

*Table 1: Mesh characteristics for cubical samples with an edge of 5 cm and computational time for non-linear diffusion of water (% indicates relative humidity).*

Mesh type in COMSOL	Normal	Fine	Finer	Extra fine	Extremely fine
Number of domain elements	16548	32433	100546	399703	217552
Number of boundary elements	1536	2412	4692	11832	35124
Number of edge elements	120	156	216	348	600
Degrees of freedom	3166	6032	17926	69372	369112
Computational time (75%)	30 seconds	51 seconds	2 minutes	9 minutes	45 minutes
Computational time (43%)	34 seconds	55 seconds	2 minutes	10 minutes	Not registered

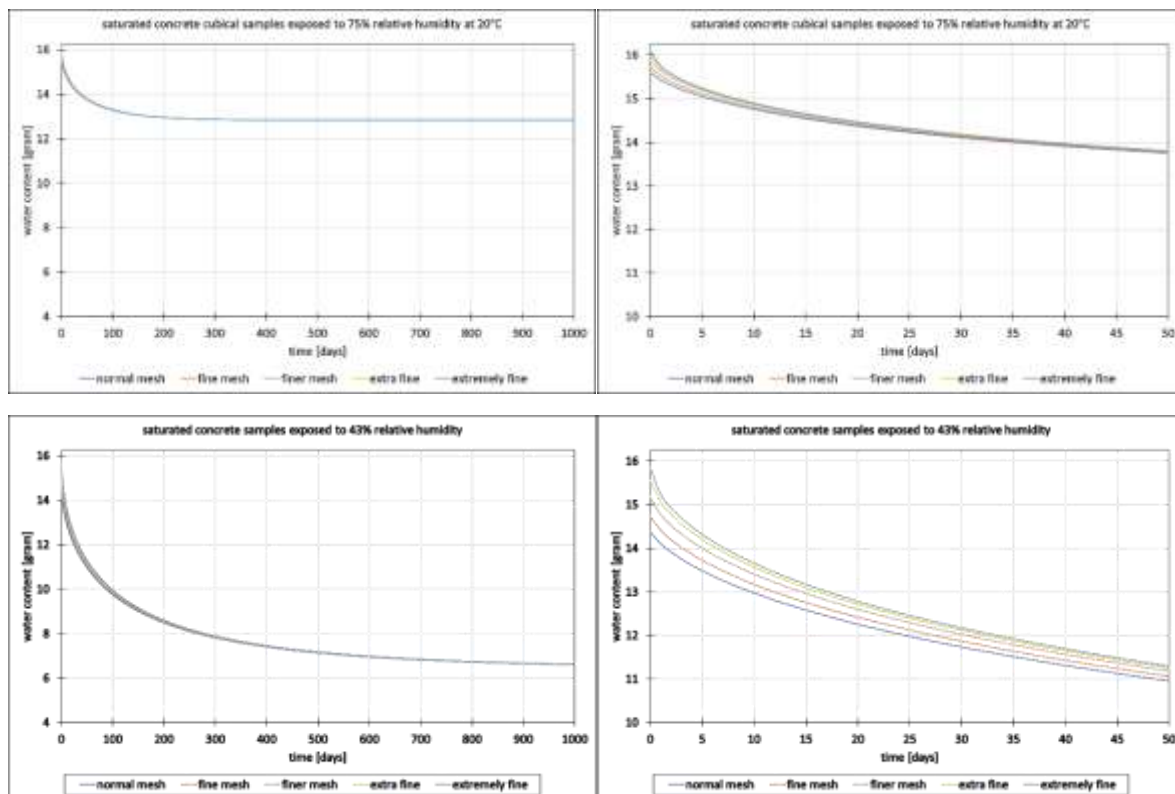
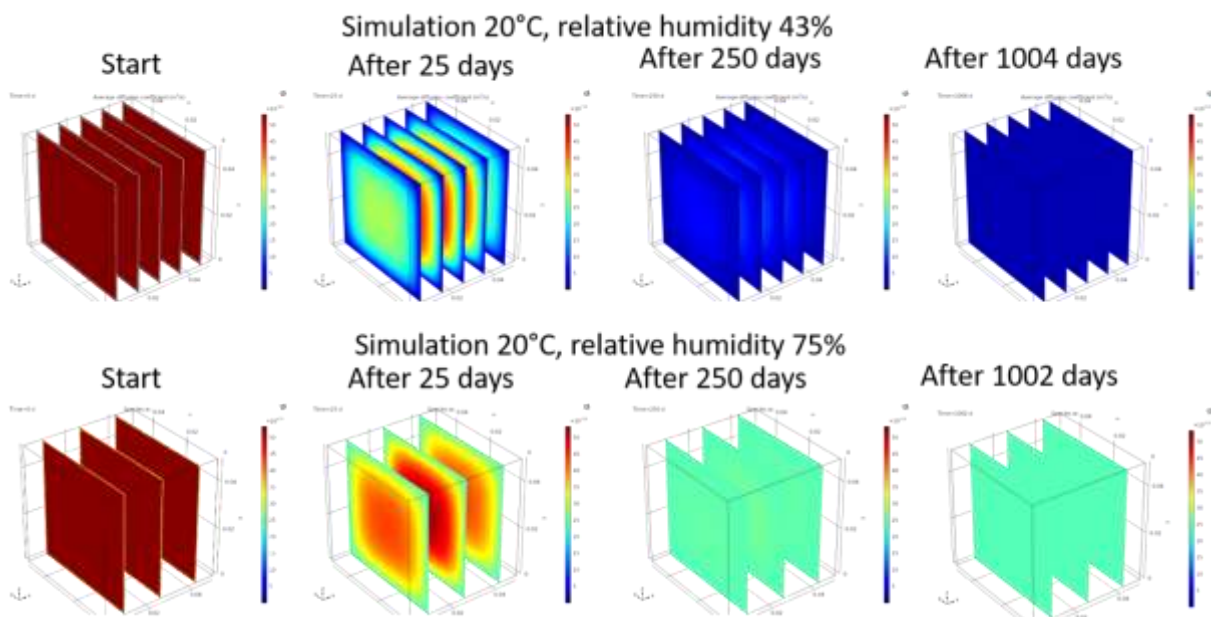


Figure 6-1: Calculated weight of water in the cubical samples for exposed to a relative humidity of 75% and 43% at different mesh densities.

The experimental error in the determination of the weight of the samples is about 0.3 to 0.4 gram. For the samples exposed to a relative humidity of 75%, the variation

between the calculated results as a function of the mesh density becomes smaller than the measurement error after 20 days. For the samples exposed to a relative humidity of 43%, the variation between the calculated results as a function of the mesh density remains larger than the measurement error after 50 days. Consequently, it depends on the experimental period and steepness of the hydraulic gradient if the calculational error is larger than this measurement error.

The calculated weights at both relative humidity's achieve a steady state but it takes a longer period in time for the samples exposed to the smallest relative humidity. The reason for this calculated feature is that the diffusion value for water becomes smaller at smaller saturation degrees in concrete. *Figure 6-1* and *Figure 6-2* show the calculated diffusion values and saturation degree as a function of time and space.



*Figure 6-2: Simulated with an extremely fine mesh, diffusion values for water in samples of COVRA's waste package as a function of time during exposure to a relative humidity of 43% and 75%. Range in linear scale: maximum  $5.3 \times 10^{-12} \text{ m}^2/\text{s}$  (dark red), minimum  $5.3 \times 10^{-15} \text{ m}^2/\text{s}$  (dark blue).*

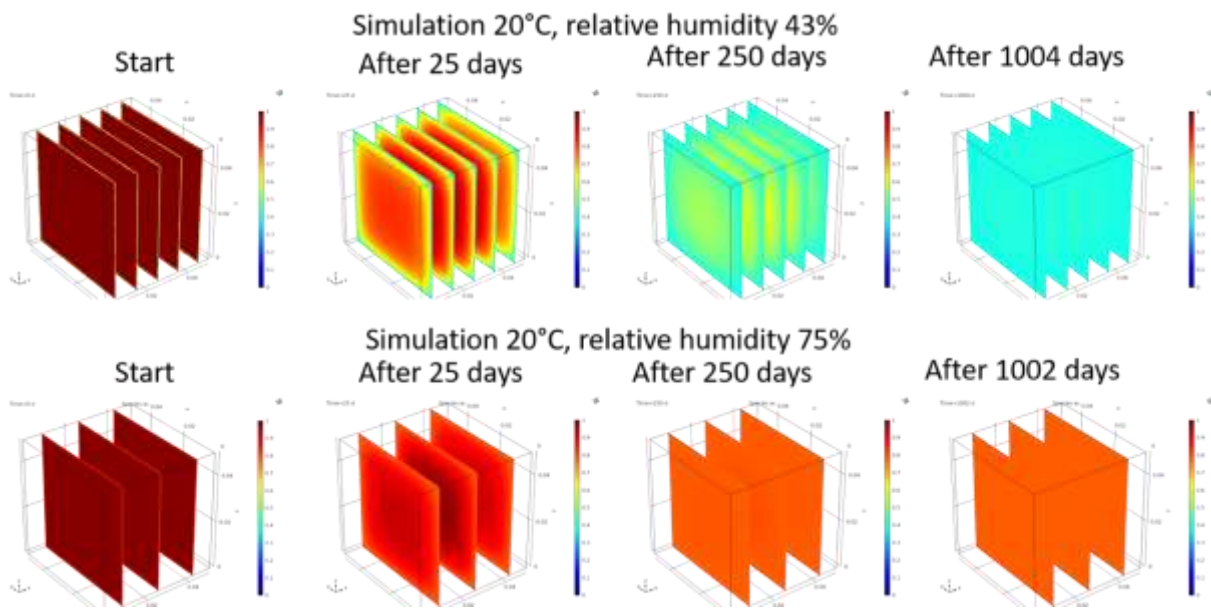


Figure 6-3: Simulated with an extremely fine mesh, saturation degrees in samples of COVRA’s waste package mortar as a function of time during exposure to a relative humidity of 43% and 75%. Range in linear scale: maximum 1 (dark red), minimum 0 (dark blue).

### 6.2.2 Transport of water and reactive gas

COVRA’s waste package mortar is made with a blended cement containing portlandite and blast furnace slag. Blast furnace slag contains traces of pyrite. These traces of pyrite react with oxygen gas; a reaction with dissolved oxygen at atmospheric conditions has not been observed within an experimental period of about 1000 days. Cementitious phase for concrete made with blast furnace slag appears to be dark blue with visible light when this pyrite is present. The oxidation of pyrite can therefore be used to validate diffusion values for reactive gases. *Figure 6-1* showed that the simulated reduction in water content of the samples takes place at a smaller rate with decreasing mesh density. Consequently, a decreasing mesh density predicts a faster disappearance of pyrite. *Figure 6-4* shows this simulated feature.

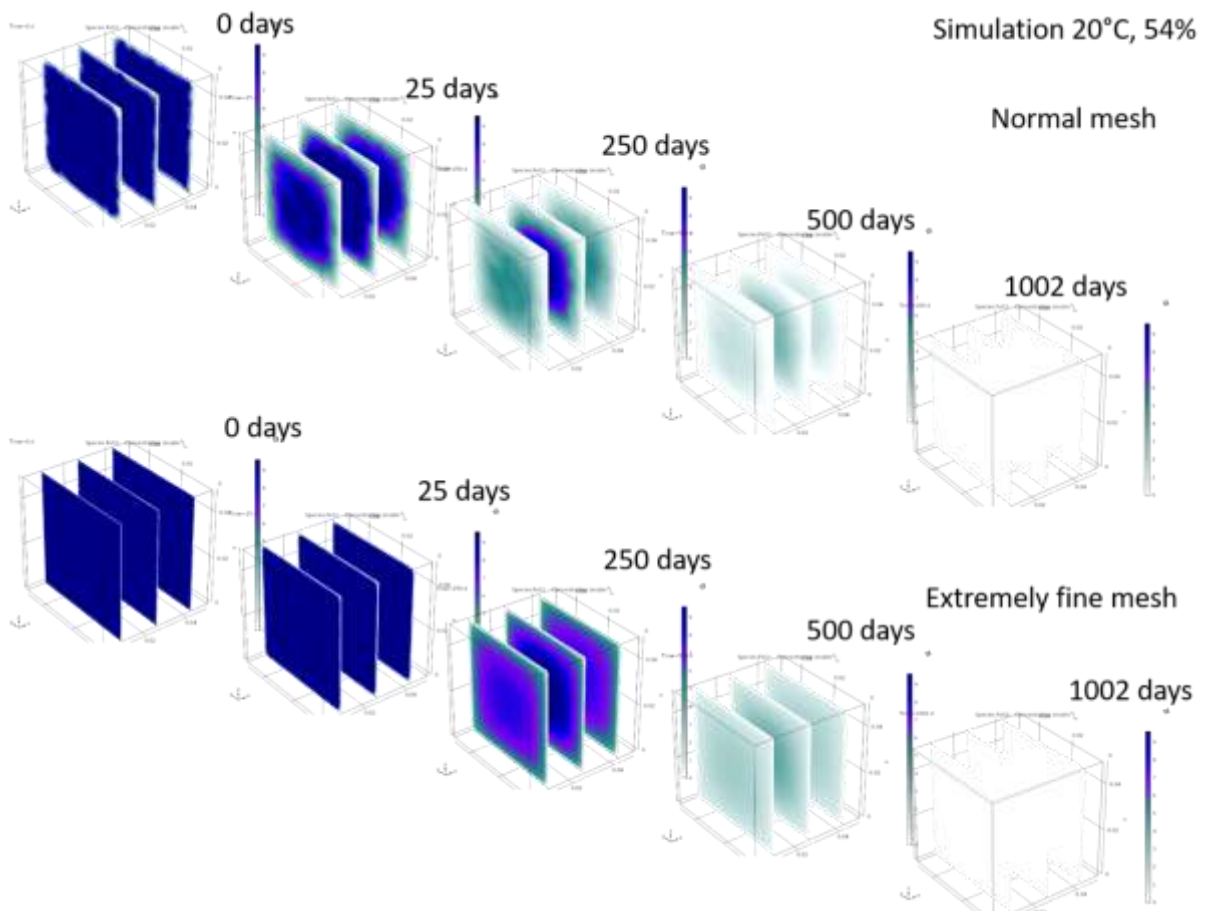


Figure 6-4: Predicted disappearance of pyrite as a function of time for a normal mesh and extremely fine mesh for initially water saturated samples that were when exposed to a relative humidity of 54%. Range in linear scale: maximum 9.6 mol  $FeS_2/m^3$  (dark blue), minimum 0 (white).

Validation of parameters used in a model with observed sharp fronts such as oxidation measured with the pyrite content and carbonation of concrete measured by spraying with a phenolphthalein solution may therefore require a high mesh density.

## 7. Appendix B: Reduced complexity and impact of discretization and convergence tolerance

### 7.1 Introduction

Águila and coworkers [78] reported a benchmark of single- and multi-species Cs sorption and diffusion through Opalinus clay. The benchmark was performed with the following codes: CORE<sup>2D</sup>V5, Flotran, COMSOL Multiphysics, OpenGeosys-GEM, MCOTAC, PHREEQC v.3 and iCP 1.5. The migration setup was solved with, i) A single-species model by using a look-up table for a cesium sorption isotherm and ii) A multi-species diffusion model including a complex mechanistic cesium cation exchange model with 3 types of exchange sites. The calculations were performed for three cesium boundary concentrations ( $10^{-3}$ ,  $10^{-5}$  and  $10^{-7}$  mol/L) to investigate the performance of the models and codes for the strongly nonlinear sorption behavior of Cs.

### 7.2 Sensitivity of computed Cs concentrations to the convergence tolerance for solving the geochemical equations

The system of chemical equations is solved with an iterative Newton-Raphson method. The unknown concentrations of the chemical components at the  $(s+1)$  iteration,  $x^{s+1}_j$ , are computed for those of the previous iteration  $x^s_j$  for  $j = 1, 2, \dots, N$ ,  $N$  being the number of unknowns. The iterative process stops when the maximum number of allowed iterations is reached or when

$$\max_j \left[ \frac{|x_j^{s+1} - x_j^s|}{(x_j^{s+1} + x_j^s)/2} \right] \leq \omega \quad (\text{B1})$$

where  $\omega$  is a prescribed convergence tolerance.

Águila et al. (2021) found that the time evolution of the computed cesium concentrations is very sensitive to the convergence tolerance ( $\omega$ ), especially for the Cs boundary concentration of  $10^{-7}$  mol/L. Several sensitivity runs were performed with CORE<sup>2D</sup>V5 to analyze the influence of  $\omega$  to solve the chemical reactions. Figure 8.1 shows the Cs breakthrough curves calculated with CORE<sup>2D</sup>V5 at  $x = 1$  and  $5$  mm by using convergence tolerances ranging from  $10^{-11}$  to  $10^{-3}$  for considering a Cs boundary concentration equal to  $10^{-7}$  mol/L. It can be seen that the curves tend to be similar when the convergence tolerance is smaller than  $10^{-6}$ .

*Figure 7-1: Sensitivity analysis of the time evolution of the Cs concentrations computed with CORE<sup>2DV5</sup> at  $x = 1$  mm (top) and at  $x = 5$  mm (bottom) by using different relative convergence tolerance ( $\omega$ ) to solve the chemical reactions. The cesium concentration at the “high” concentration boundary is equal to  $10^{-7}$  mol/L [78].*

### 7.3 Conclusions

Generally, good agreement for both single- and multi-species benchmark concepts was achieved (see Fig. 8.2). However, some discrepancies were found, especially near the boundaries where code-specific spatial and temporal discretization had to be improved to ensure a good agreement at the expense of longer computation times. In addition, the benchmark exercise yielded useful information on code performance, setup options, input and output data management, and post-processing options. The comparison of the single-species and multi-species model concepts showed that the single-species model yielded generally an earlier breakthrough because the latter accounts neither for cation exchange of  $\text{Cs}^+$  with  $\text{K}^+$  and  $\text{Na}^+$  nor for  $\text{K}^+$  and  $\text{Na}^+$  diffusion in the pore water.

Good agreement was obtained in all cases for the single-species model. Small differences could be attributed to different discretization, different implementation of the sorption isotherm and different interpolation procedures used by the codes. Sensitivity analysis performed with CORE<sup>2DV5</sup>, MCOTAC and OpenGeosys-GEM showed the importance of spatial discretization on the computed results. The use of too coarse grids generally adds a lot of “numerical dispersion”.

Some discrepancies were found for the complex multi-species Cs sorption model with cation exchange on three sorption sites. They were attributed to differences in the spatial discretization, time stepping and the implementation of the boundary conditions.

The comparison of the model results computed with the single-species and the multi-species complex Cs sorption models showed that the single-species model yielded a Cs breakthrough faster than that of the multi-species model. It should be taken into account that the single-species model does not consider the cation exchange of  $\text{Cs}^+$  with  $\text{K}^+$  and  $\text{Na}^+$  and the diffusion of dissolved  $\text{K}^+$  and  $\text{Na}^+$ .

The main difference between the single species and the multispecies reactive transport models is the computation time. The computation time of the single species model is at least 25 times smaller than that of the multi-species model. Although this can be seen as a clear advantage for the use of the single species model for the long-term prediction of radionuclides migration, the multi-species model provides a better and deeper understanding of the geochemistry of the system.

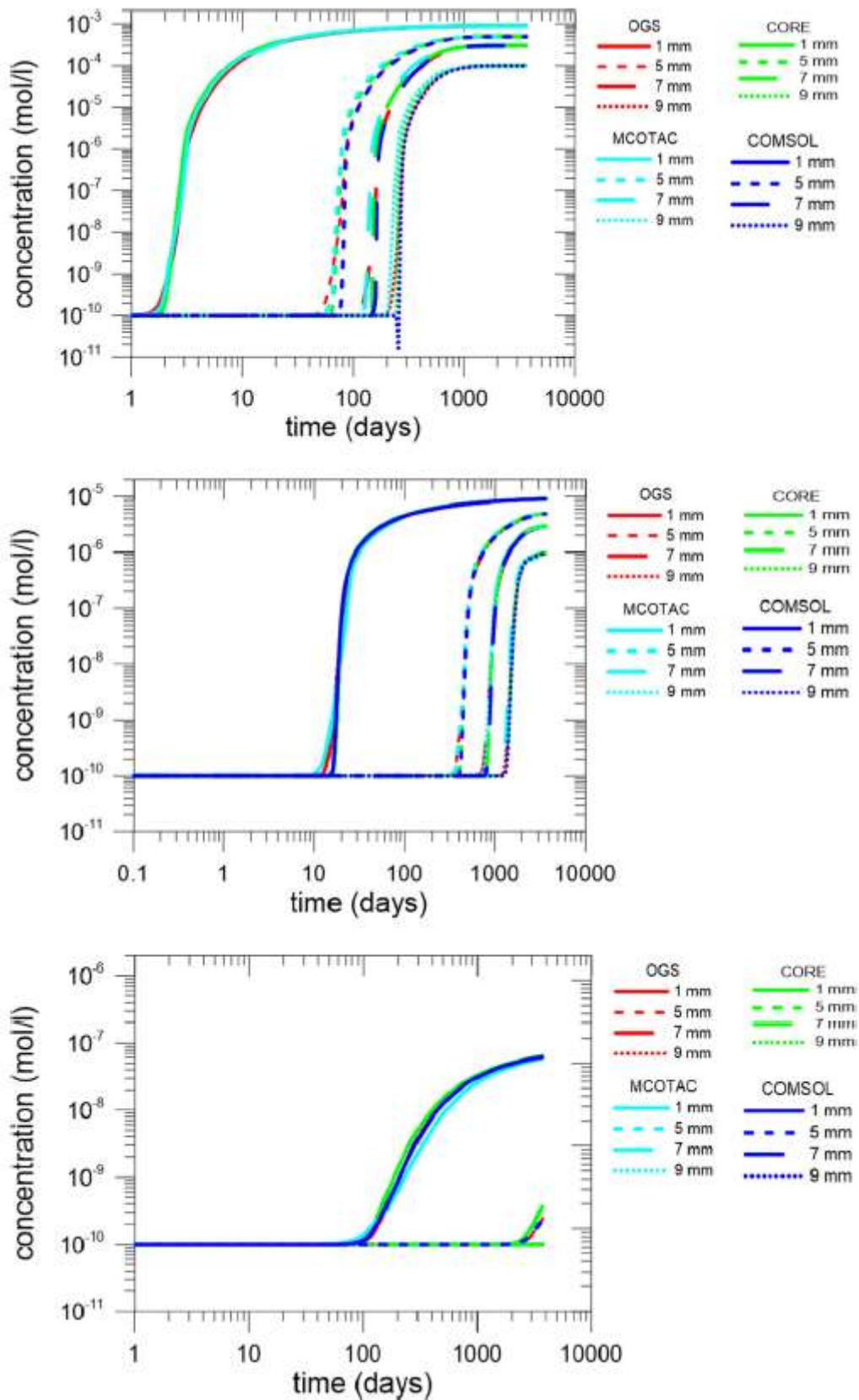


Figure 7-2: Cs breakthrough curves calculated with the multi-species transport models at different locations in the Opalinus clay samples by using five reactive

*transport codes. The cesium concentration at the “high” concentration boundary are equal to  $10^{-3}$  mol/L (top),  $10^{-5}$  mol/L (middle) and  $10^{-7}$  mol/L (bottom).*

## 8. Appendix C: Reduced dimensionality in axi-symmetric models

### 8.1 Introduction

The reference concept for HLW disposal in horizontal galleries allows for consideration of axial symmetry for water flow, heat and reactive solute transport.

This appendix presents two examples, which illustrate the reduction in dimensions from fully 3D to 3D axi-symmetric to 2D axi-symmetric.

### 8.2 Febex in situ test

FEBEX (Full-scale Engineered Barrier EXperiment) was a demonstration and research project dealing with the engineered barrier system designed for sealing and containment of a radioactive waste repository ([79], [80]). FEBEX was based on the Spanish reference concept for the disposal of radioactive waste in crystalline rocks. The FEBEX in situ test was performed in two operation periods. The 1st period lasted from 1997 to 2002 when the first half of the experiment around heater 1 was dismantled. Heater 2 was switched off and the full test was dismantled in 2015 (*Figure 8-1*).

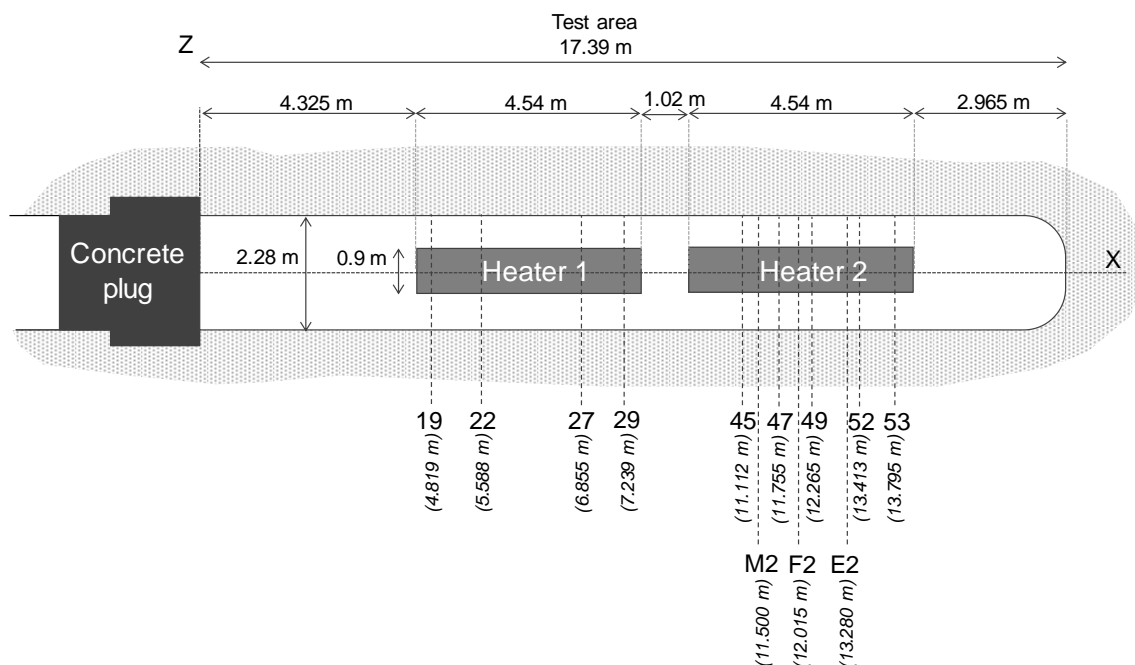


Figure 8-1: General layout of the FEBEX in situ test, taken from [80].

The geometry of the FEBEX in situ test tends to favour that the thermal, hydrodynamic and chemical processes exhibit axial symmetry with respect to the axis of the gallery

in sections far from the ends of the heaters. The interactions with the cooler sections at the ends of the heaters impair the axial symmetry assumption far from the heaters.

This experiment was modelled by using 1D and 2D axisymmetric models. The computed temperatures, relative humidities, water contents and pore water pressures computed with 1D and 2D models show some differences. The differences in the computed temperatures are generally small (*Figure 8-2*), but those of the computed water content are significant (*Figure 8-3*).

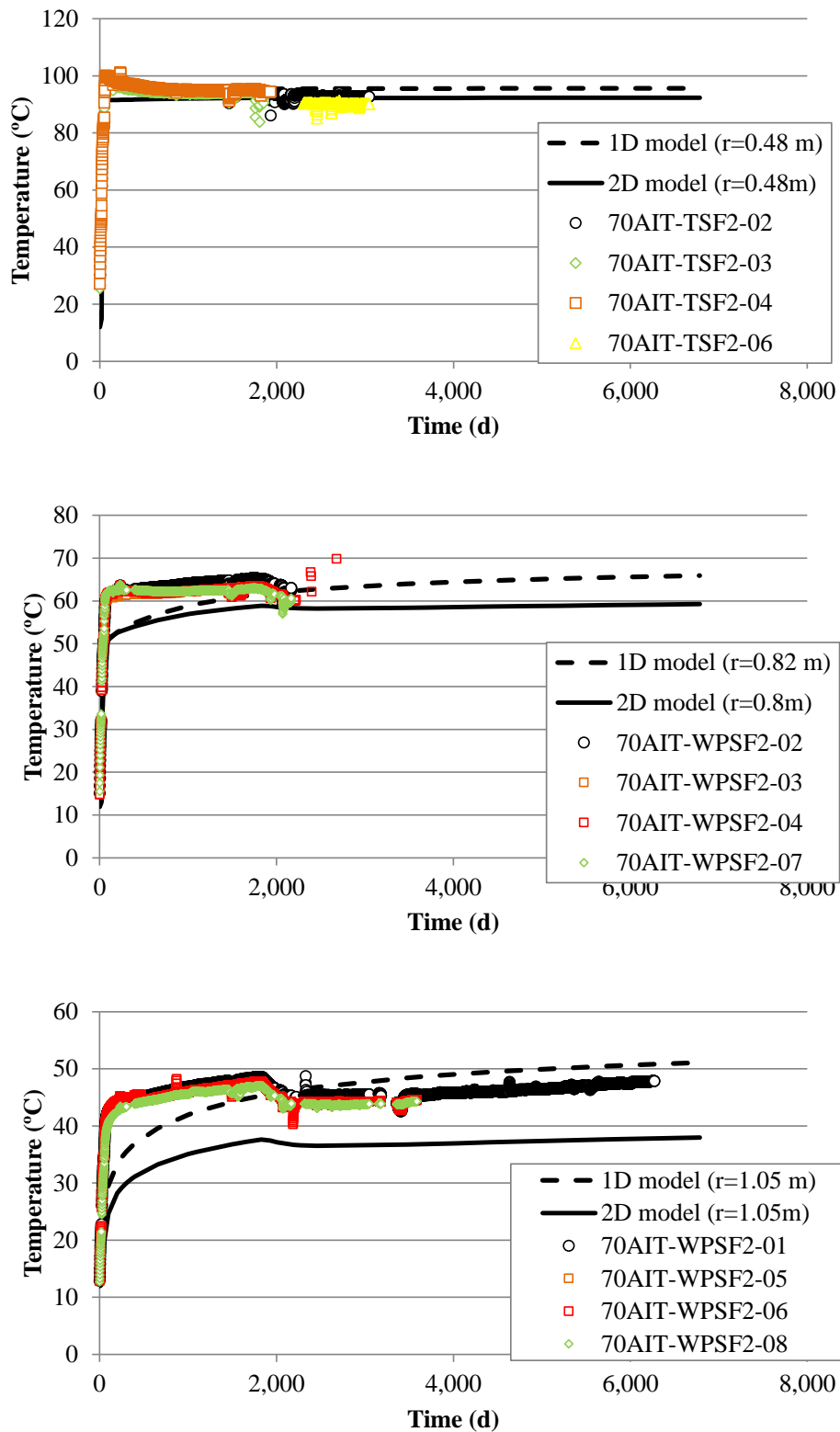


Figure 8-2: Time evolution of the calculated temperatures (lines) with the 1D and 2D axisymmetric models and the measured temperatures (symbols) in a hot section at radial distances  $r = 0.48\text{ m}$ ,  $r = 0.82\text{ m}$  and  $r = 1.05\text{ m}$  taken from [79].

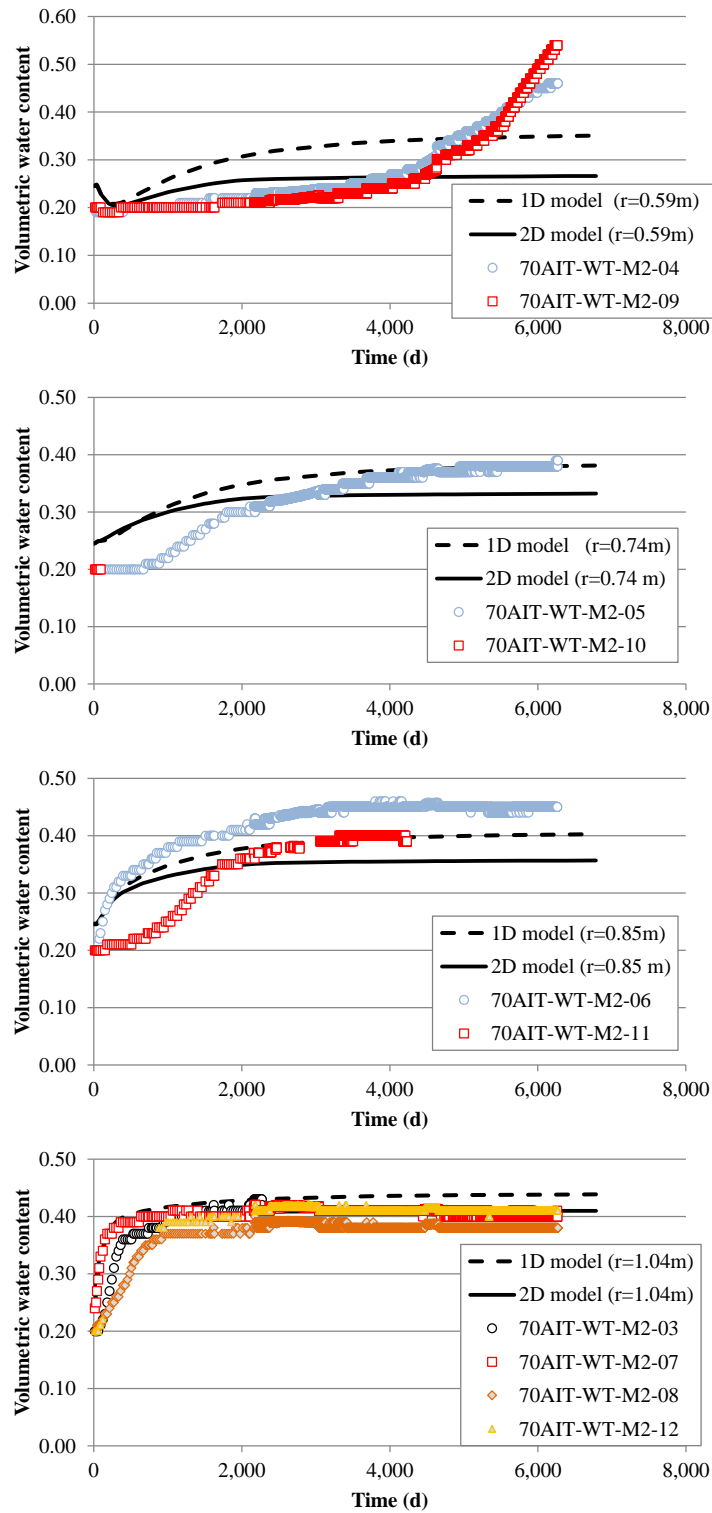


Figure 8-3: Time evolution of the computed water content (lines) with the 1D and 2D axisymmetric models and measured data (symbols) in a hot section taken from [79].

The concentrations of dissolved  $\text{Cl}^-$  in 2002 are large near the heaters 1 and 2. The largest concentrations are located at the edge of heater 2. The contour lines are approximately parallel to the axis of the gallery along heaters 1 and 2. In the edges of the heaters, however, the contour lines are no longer parallel to the gallery axis. The computed contour plots of  $\text{Cl}^-$  concentrations illustrate that the edge effects extend approximately over a distance of 0.5 to 1 m (*Figure 8-4*). The concentrations of  $\text{Cl}^-$  in 2015 show a significant decrease compared to the concentrations in 2002 around heater 2. Large concentrations of  $\text{Cl}^-$  still remain in the bentonite barrier between the dummy and heater 2 and between heater 2 and the end of the gallery.

The concentrations of  $\text{Cl}^-$  computed with the 1D axisymmetric model in a hot section in 2015 are smaller than the concentrations calculated with the 2D model because the bentonite hydration rate calculated with the 1D axisymmetric model is slightly larger than the hydration calculated with the 2D model. The concentrations calculated in a cold section with the 1D axisymmetric model are significantly smaller than the concentrations computed with the 2D axisymmetric model.

j

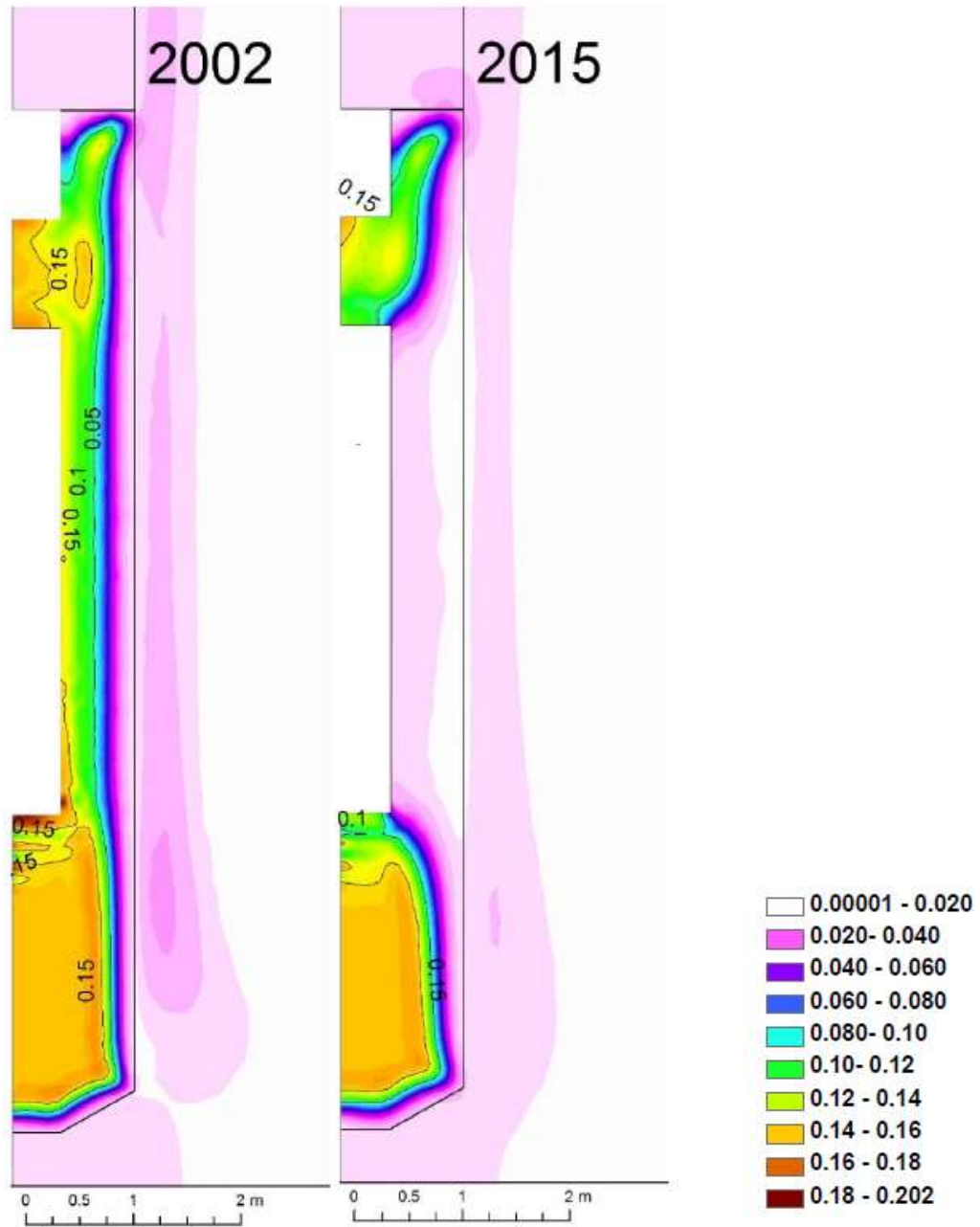


Figure 8-4: Contour plots of the computed Cl<sup>-</sup> concentrations at dismantling times of Heater #1 in 2002 (left) and Heater #2 in 2015 (right) taken from [79].

### 8.3 1D and 2D axi-symmetric models for a HLW repository in granite

In [81] 1-D and 2-D axisymmetric water flow and multicomponent reactive solute transport models were presented to simulate the long-term hydrochemical evolution of porewater composition in the near field of a repository in fractured granite. The models consider canister corrosion and the interactions of corrosion products with bentonite.

The 1-D and 2-D axisymmetric models share the same radial discretization scheme. The 2-D axisymmetric model accounts for groundwater flow through the EDZ and the granite by assuming that groundwater flow is parallel to the galleries (*Figure 8-5*). The model domain extends 25 m along the radial direction,  $x$ , and 6.5 m along the longitudinal direction,  $y$ . The total flow rate is 4.59 L/y. The model accounts for an excavation damaged zone (EDZ) zone with a hydraulic conductivity an order of magnitude larger than that of granite.

The 1-D model has 200 nodes and 199 elements (see *Figure 8-6*). The 2-D model has 994 nodes and 1820 triangular elements. Numerical simulations were performed at a constant temperature of 25 °C for a time horizon of 0.3 Ma.

The 2-D model of canister corrosion was performed with the model of progressive corrosion which assumes that corrosion takes place at  $t = 0$  only at the canister-bentonite interface ( $x = 0.45$  m). Later, corrosion progresses inwards. A constant corrosion rate of 0.2  $\mu\text{m/y}$  was adopted. Sensitivity runs were performed to evaluate model uncertainties. Since the 2-D axisymmetric model with progressive corrosion requires a large computation time, sensitivity runs were performed with a simplified 1-D axisymmetric model without flow in granite and by assuming that corrosion takes place everywhere in the canister. Sensitivity runs were performed to changes in: 1) Corrosion rate; 2) Proton surface complexation; and 3) Iron sorption via surface complexation.

Samper et al. [82] found that the 1-D model provides similar results to those of the 2-D model, but the 1-D model requires half of the CPU time. A 1-D axisymmetric model without groundwater flow was used to evaluate the changes in porosity, which were calculated to be small and have no significant effect on the geochemical evolution of the system.

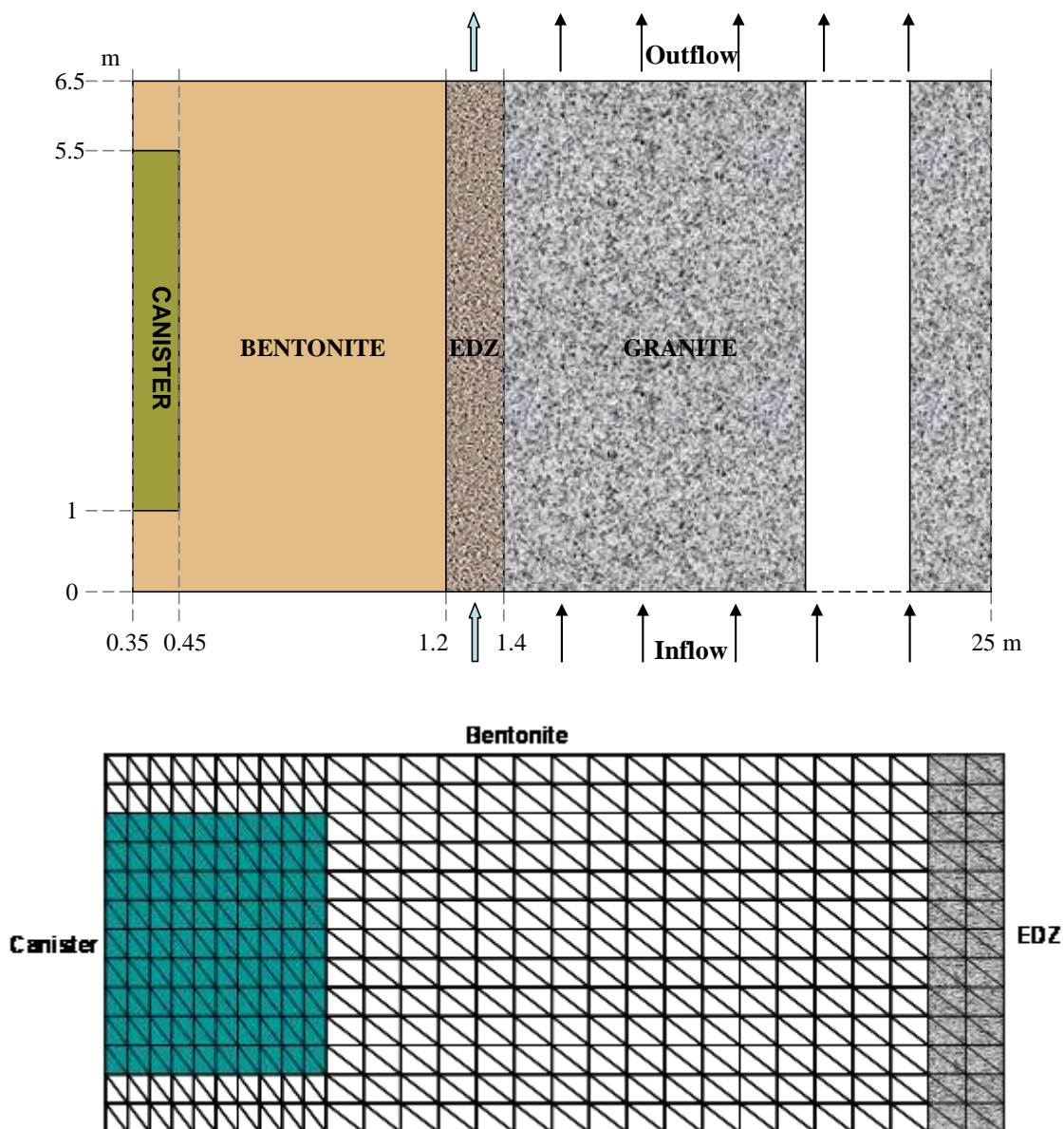


Figure 8-5: Geometry and material zones of the 2-D axisymmetric model (top) and zoom of the canister-bentonite-EDZ (bottom) taken from [82].

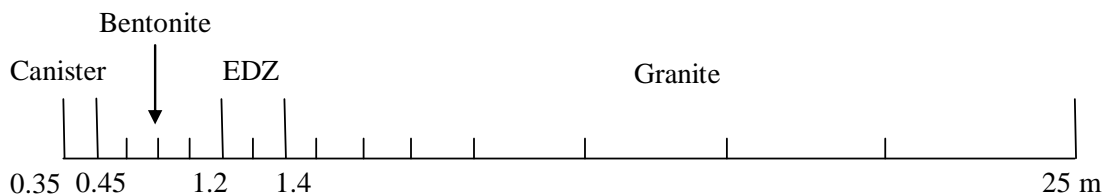


Figure 8-6: Finite element mesh used in the 1-D axisymmetric model [82].

Magnetite is the main corrosion product. Figure 9-7 shows the computed spatial distribution of the cumulative canister corrosion and magnetite precipitation after  $10^5$

and  $2 \cdot 10^5$  years. Most of the Fe diffuses from the canister into the bentonite where it precipitates. Siderite precipitation is two orders of magnitude smaller than magnetite precipitation due to the limited availability of dissolved carbonates. The amounts of dissolved, sorbed and exchanged iron are two orders of magnitude smaller than that of precipitated siderite. Bentonite porosity decreases due to magnetite precipitation. The apparent distribution coefficient,  $K_d$ , of corrosion products derived from computed dissolved and exchanged Fe concentrations increases strongly with time, indicating that the use of a constant  $K_d$  for corrosion products is largely unrealistic. Proton surface complexation is highly effective in buffering pH in bentonite porewater, which increases due to canister corrosion. Other mechanisms such as calcite dissolution/precipitation, Fe exchange and dissolution/precipitation of Fe minerals are much less effective in buffering pH.

The computed  $\text{Cl}^-$  concentration of dissolved  $\text{Cl}^-$  in the bentonite ( $r = 0.8$  m) is very sensitive to the groundwater flow,  $Q$ . It should be noticed that the 2-D with no groundwater flow and the 1-D model provide identical results. Dissolved  $\text{Cl}^-$  diffuses from the bentonite into the granite where groundwater flow transports it away from bentonite. Therefore, the larger  $Q$  the faster the concentration of dissolved  $\text{Cl}^-$  decreases in the bentonite.

The main conclusions of this case include:

- 1) A 1-D axisymmetric model without groundwater was used because it requires half of the CPU time of the 2D model.
- 2) Sensitivity analyses and detailed analyses of porosity clogging near the canister were evaluated with the 1D model
- 3) The 1-D model provides identical results to those of the 2-D model when the groundwater flow through the granite is very small. Otherwise, the computed concentrations of dissolved species with the 2D axisymmetric model differ from those of the 1D model

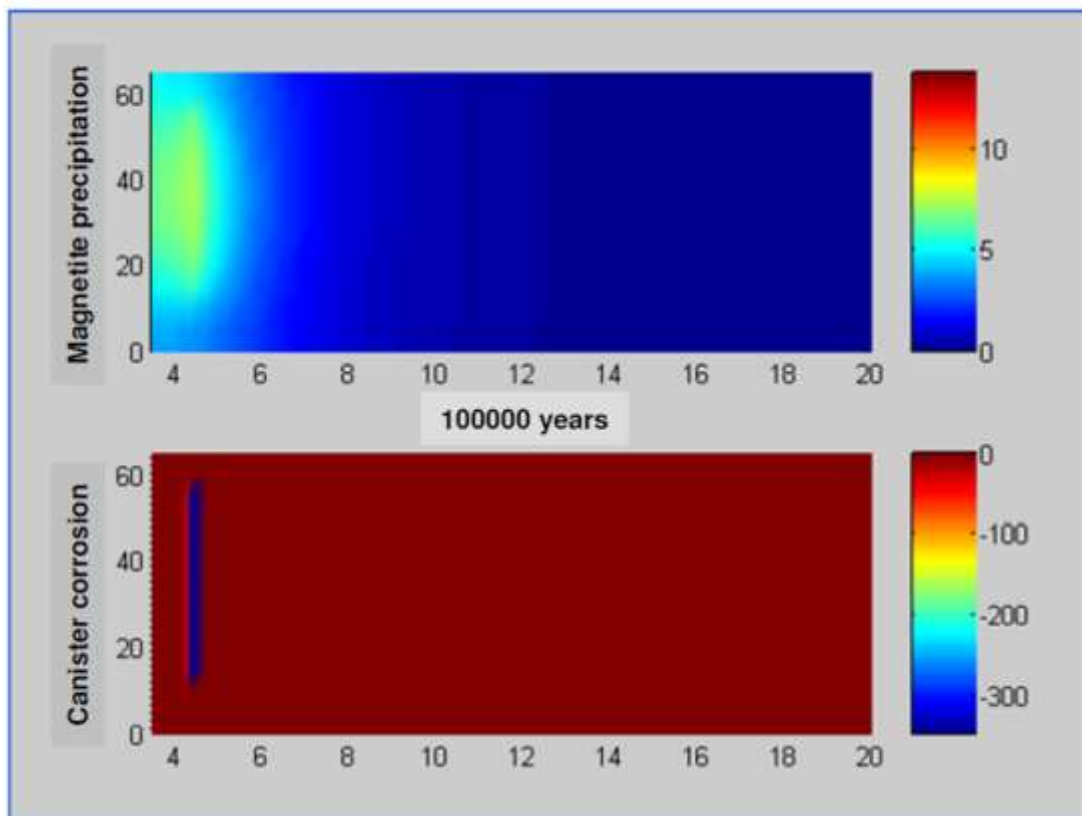


Figure 8-7: Computed spatial distribution of the cumulative canister corrosion and magnetite precipitation after  $10^5$  years (top) and  $2 \cdot 10^5$  years (bottom) (units: mol/L) [82].

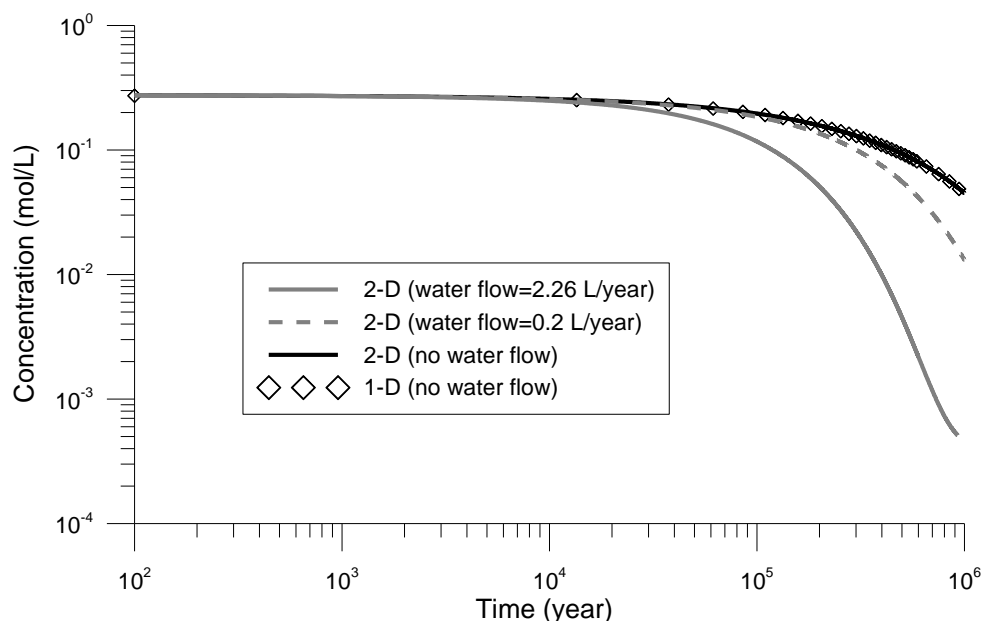


Figure 8-8: Sensitivity of the computed  $Cl^-$  concentration of dissolved  $Cl^-$  in the bentonite ( $r = 0.8$  m) to groundwater flow. It should be noticed that 2-D model with no flow and the 1-D model provide identical results [82].

## References

- [1] F. K. Frantz, “Taxonomy of model abstraction techniques,” 1995, doi: 10.1145/224401.224834.
- [2] S. Razavi, B. A. Tolson, and D. H. Burn, “Review of surrogate modeling in water resources,” *Water Resources Research*. 2012, doi: 10.1029/2011WR011527.
- [3] J. E. M. Baartman, L. A. Melsen, D. Moore, and M. J. van der Ploeg, “On the complexity of model complexity: Viewpoints across the geosciences,” *Catena*, vol. 186, no. September 2019, p. 104261, 2020, doi: 10.1016/j.catena.2019.104261.
- [4] O. Bildstein, F. Claret, and P. Frugier, “RTM for Waste Repositories,” *Rev. Mineral. Geochemistry*, vol. 85, no. 1, pp. 419–457, 2019, doi: 10.2138/rmg.2019.85.14.
- [5] A. Saltelli *et al.*, *Global Sensitivity Analysis. The Primer*. 2008.
- [6] Y. A. Pachepsky *et al.*, “Model Abstraction Techniques for Soil-Water Flow and Transport,” *Office*, p. NUREG/CR-6884, 2006.
- [7] I. Berre, F. Doster, and E. Keilegavlen, “Flow in Fractured Porous Media: A Review of Conceptual Models and Discretization Approaches,” *Transp. Porous Media*, vol. 130, no. 1, pp. 215–236, 2019, doi: 10.1007/s11242-018-1171-6.
- [8] R. Liu, B. Li, Y. Jiang, and N. Huang, “Review: Mathematical expressions for estimating equivalent permeability of rock fracture networks,” *Hydrogeol. J.*, vol. 24, no. 7, 2016, doi: 10.1007/s10040-016-1441-8.
- [9] J. E. Warren and P. J. Root, “The Behavior of Naturally Fractured Reservoirs,” *Soc. Pet. Eng. J.*, vol. 3, no. 03, pp. 245–255, Sep. 1963, doi: 10.2118/426-pa.
- [10] K. Pruess, “Brief guide to the MINC-Method for modeling flow and transport in fractured media,” *Lbl-32195*, pp. 1–15, May 1992, doi: 10.2172/6951290.
- [11] P. C. Lichtner, “Critique of dual continuum formulations of multicomponent reactive transport in fractured porous media,” in *Geophysical Monograph Series*, vol. 122, Blackwell Publishing Ltd, 2000, pp. 281–298.
- [12] A. Iraola, P. Trinchero, S. Karra, and J. Molinero, “Assessing dual continuum method for multicomponent reactive transport,” *Comput. Geosci.*, vol. 130, pp. 11–19, Sep. 2019, doi: 10.1016/j.cageo.2019.05.007.
- [13] R. Haggerty and S. M. Gorelick, “Multiple-Rate Mass Transfer for Modeling Diffusion and Surface Reactions in Media with Pore-Scale Heterogeneity,” *Water Resour. Res.*, vol. 31, no. 10, pp. 2383–2400, 1995, doi: 10.1029/95WR10583.
- [14] T. Babey, J. R. de Dreuzy, and C. Casenave, “Multi-Rate Mass Transfer (MRMT) models for general diffusive porosity structures,” *Adv. Water Resour.*, vol. 76, no. December, pp. 146–156, 2015, doi: 10.1016/j.advwatres.2014.12.006.
- [15] R. Therrien and E. A. Sudicky, “Three-dimensional analysis of variably-saturated flow and solute transport in discretely-fractured porous media,” *J. Contam. Hydrol.*, vol. 23, no. 1–2, pp. 1–44, Jun. 1996, doi: 10.1016/0169-7722(95)00088-7.

- [16] B. Flemisch *et al.*, “Benchmarks for single-phase flow in fractured porous media,” *Adv. Water Resour.*, vol. 111, pp. 239–258, Jan. 2018, doi: 10.1016/j.advwatres.2017.10.036.
- [17] A. Fumagalli, E. Keilegavlen, and S. Scialò, “Conforming, non-conforming and non-matching discretization couplings in discrete fracture network simulations,” *J. Comput. Phys.*, vol. 376, pp. 694–712, Jan. 2019, doi: 10.1016/j.jcp.2018.09.048.
- [18] A. Moinfar, A. Varavei, K. Sepehrnoori, and R. T. Johns, “Development of an efficient embedded discrete fracture model for 3D compositional reservoir simulation in fractured reservoirs,” *SPE J.*, vol. 19, no. 2, pp. 289–303, Apr. 2014, doi: 10.2118/154246-PA.
- [19] C. I. Steefel and C. Tournassat, “A model for discrete fracture-clay rock interaction incorporating electrostatic effects on transport,” *Comput. Geosci.*, 2020, doi: 10.1007/s10596-020-10012-3.
- [20] T. Hennig and M. Kühn, “Surrogate model for multi-component diffusion of uranium through opalinus clay on the host rock scale,” *Appl. Sci.*, vol. 11, no. 2, pp. 1–21, 2021, doi: 10.3390/app11020786.
- [21] B. Arora, J. A. Davis, N. F. Spycher, W. Dong, and H. M. Wainwright, “Comparison of Electrostatic and Non-Electrostatic Models for U(VI) Sorption on Aquifer Sediments,” *Groundwater*, 2018, doi: 10.1111/gwat.12551.
- [22] A. Idiart *et al.*, “Reactive transport modelling of a low-pH concrete / clay interface,” *Appl. Geochemistry*, vol. 115, 2020, doi: 10.1016/j.apgeochem.2020.104562.
- [23] A. Idiart and B. Shafei, “Modelling of concrete degradation - Hydrochemical processes. Report for the safety evaluation SE-SFL (SKB R-19-11),” 2019.
- [24] P. E. Mariner, T. M. Berg, K. W. Chang, B. J. Debusschere, R. C. Leone, and D. T. Seidl, “Surrogate Model Development of Spent Fuel Degradation for Repository Performance Assessment Spent Fuel and Waste Disposition (SAND2020-10797 R),” 2020.
- [25] COMSOL Multiphysics®, *version 5.6*. Stockholm, Sweden: COMSOL AB.
- [26] S. Finsterle, R. A. Muller, J. Grimsich, J. Apps, and R. Baltzer, “Post-closure safety calculations for the disposal of spent nuclear fuel in a generic horizontal drillhole repository,” *Energies*, vol. 13, no. 10, 2020, doi: 10.3390/en13102599.
- [27] L. O. Höglund, “The impact of concrete degradation on the BMA barrier functions,” 2014.
- [28] J. F. Águila, J. Samper, A. Mon, and L. Montenegro, “Dynamic update of flow and transport parameters in reactive transport simulations of radioactive waste repositories,” *Appl. Geochemistry*, vol. 117, p. 104585, Jun. 2020, doi: 10.1016/J.APGEOCHEM.2020.104585.
- [29] A. Saltelli, S. Tarantola, F. Campolongo, and M. Ratto, *Sensitivity Analysis in Practice*. 2002.
- [30] E. Borgonovo, *Sensitivity Analysis: An Introduction for the Management Scientist*. 2017.
- [31] E. Borgonovo and E. Plischke, “Sensitivity analysis: A review of recent

- advances,” *European Journal of Operational Research*. 2016, doi: 10.1016/j.ejor.2015.06.032.
- [32] R. Ghanem, H. Owhadi, and D. Higdon, *Handbook of uncertainty quantification*. 2017.
- [33] I. M. Sobol, “Sensitivity analysis for non-linear mathematical models,” *Math. Model. Comput. Exp.*, 1993.
- [34] A. Saltelli, P. Annoni, I. Azzini, F. Campolongo, M. Ratto, and S. Tarantola, “Variance based sensitivity analysis of model output. Design and estimator for the total sensitivity index,” *Comput. Phys. Commun.*, 2010, doi: 10.1016/j.cpc.2009.09.018.
- [35] K. Chan, A. Saltelli, and S. Tarantola, “Winding stairs: A sampling tool to compute sensitivity indices,” *Stat. Comput.*, 2000, doi: 10.1023/A:1008950625967.
- [36] E. J. Bonano and R. M. Cranwell, “Treatment of uncertainties in the performance assessment of geologic high-level radioactive waste repositories,” *Math. Geol.* 1988 205, vol. 20, no. 5, pp. 543–565, Jul. 1988, doi: 10.1007/BF00890336.
- [37] J. C. Helton, C. W. Hansen, and C. J. Sallaberry, “Uncertainty and sensitivity analysis in performance assessment for the proposed high-level radioactive waste repository at Yucca Mountain, Nevada,” *Reliab. Eng. Syst. Saf.*, vol. 107, pp. 44–63, Nov. 2012, doi: 10.1016/J.RESS.2011.07.002.
- [38] J. C. Helton and C. J. Sallaberry, “Treatment of uncertainty in performance assessments for the geological disposal of radioactive waste,” *Geol. Repos. Syst. Safe Dispos. Spent Nucl. Fuels Radioact. Waste*, pp. 499–527, Jun. 2017, doi: 10.1016/B978-0-08-100642-9.00017-7.
- [39] M. Matsumoto and A. Neyama, “Uncertainty Analysis Tool for the Performance Assessment of the High Level Radioactive Waste Disposal System,” *Int. Conf. Nucl. Eng. Proceedings, ICONE*, vol. 2, pp. 145–152, Jun. 2009, doi: 10.1115/ICONE16-48765.
- [40] L. J. Criscenti, G. F. Laniak, and R. L. Erikson, “Propagation of uncertainty through geochemical code calculations,” *Geochim. Cosmochim. Acta*, vol. 60, no. 19, pp. 3551–3568, Oct. 1996, doi: 10.1016/0016-7037(96)00188-3.
- [41] F. H. Denison and J. Garnier-Laplace, “The effects of database parameter uncertainty on uranium(VI) equilibrium calculations,” *Geochim. Cosmochim. Acta*, vol. 69, no. 9, pp. 2183–2191, May 2005, doi: 10.1016/J.GCA.2004.09.033.
- [42] G. Ceriotti, G. M. Porta, C. Geloni, M. Dalla Rosa, and A. Guadagnini, “Quantification of CO<sub>2</sub> generation in sedimentary basins through carbonate/clays reactions with uncertain thermodynamic parameters,” *Geochim. Cosmochim. Acta*, vol. 213, pp. 198–215, Sep. 2017, doi: 10.1016/J.GCA.2017.06.015.
- [43] A. Ayoub, W. Pflingsten, L. Podofillini, and G. Sansavini, “Uncertainty and sensitivity analysis of the chemistry of cesium sorption in deep geological repositories,” *Appl. Geochemistry*, vol. 117, Jun. 2020, doi: 10.1016/J.APGEOCHEM.2020.104607.
- [44] M. Hayek, B. S. RamaRao, and M. Lavenue, “An Adjoint Sensitivity Model for

- Transient Sequentially Coupled Radionuclide Transport in Porous Media,” *Water Resour. Res.*, vol. 56, no. 7, p. e2020WR027274, Jul. 2020, doi: 10.1029/2020WR027274.
- [45] M. Hayek, B. S. RamaRao, and M. Lavenue, “An Adjoint Sensitivity Model for Steady-State Sequentially Coupled Radionuclide Transport in Porous Media,” *Water Resour. Res.*, vol. 55, no. 11, pp. 8800–8820, Nov. 2019, doi: 10.1029/2019WR025686.
- [46] A. Saltelli, M. Ratto, S. Tarantola, and F. Campolongo, “Sensitivity analysis for chemical models,” *Chemical Reviews*. 2005, doi: 10.1021/cr040659d.
- [47] A. Saltelli, M. Ratto, S. Tarantola, and F. Campolongo, “Update 1 of: Sensitivity analysis for chemical models,” *Chemical Reviews*. 2012, doi: 10.1021/cr200301u.
- [48] C. A. Holle, B. Ahmmed, V. V Vesselinov, and S. C. James, “Developing a machine learning framework to reduce the computational burden of reactive-transport simulations,” *AGU Fall Meet.*, no. December, p. 1, 2019, doi: 10.13140/RG.2.2.30319.79527.
- [49] R. Khan, “Evaluation of the Geologic CO<sub>2</sub> Sequestration Potential of the Morrow B Sandstone in the Farnsworth , Texas Hydrocarbon Field using Reactive Transport Modeling,” 2017.
- [50] N. I. Prasianakis, R. Haller, M. Mahrous, J. Poonosamy, W. Pflingsten, and S. V. Churakov, “Neural network based process coupling and parameter upscaling in reactive transport simulations,” *Geochim. Cosmochim. Acta*, vol. 291, pp. 126–143, 2020, doi: 10.1016/j.gca.2020.07.019.
- [51] S. Whitaker, “Diffusion and dispersion in porous media,” *AIChE J.*, vol. 13, no. 3, pp. 420–427, May 1967, doi: 10.1002/aic.690130308.
- [52] U. Hornung, *Homogenization and Porous Media*, vol. 98, no. 3. 1991.
- [53] B. Noetinger, “The effective permeability of a heterogeneous porous medium,” *Transp. Porous Media*, vol. 15, no. 2, pp. 99–127, 1994, doi: 10.1007/BF00625512.
- [54] S. Hanasoge, U. Agarwal, K. Tandon, and J. M. V. A. Koelman, “Renormalization group theory outperforms other approaches in statistical comparison between upscaling techniques for porous media,” *Phys. Rev. E*, vol. 96, no. 3, 2017, doi: 10.1103/PhysRevE.96.033313.
- [55] B. D. Wood, F. Cherblanc, M. Quintard, and S. Whitaker, “Volume averaging for determining the effective dispersion tensor: Closure using periodic unit cells and comparison with ensemble averaging,” *Water Resour. Res.*, vol. 39, no. 8, 2003, doi: 10.1029/2002WR001723.
- [56] B. Noetinger and T. Estebenet, “Up-scaling of double porosity fractured media using continuous-time random walks methods,” *Transp. Porous Media*, vol. 39, no. 3, 2000, doi: 10.1023/A:1006639025910.
- [57] N. I. Prasianakis, M. Gatschet, A. Abbasi, and S. V. Churakov, “Upscaling strategies of porosity-permeability correlations in reacting environments from pore-scale simulations,” *Geofluids*, vol. 2018, pp. 1–9, 2018, doi: 10.1155/2018/9260603.

- [58] M. Repina, F. Bouyer, and V. Lagneau, “Reactive transport modeling of glass alteration in a fractured vitrified nuclear glass canister: From upscaling to experimental validation,” *J. Nucl. Mater.*, 2020, doi: 10.1016/j.jnucmat.2019.151869.
- [59] J. H. Ferziger and M. Perić, *Computational Methods for Fluid Dynamics / J.H. Ferziger, M. Peric.* 2002.
- [60] C. J. Roy, “Review of discretization error estimators in scientific computing,” 2010, doi: 10.2514/6.2010-126.
- [61] P. K. Davis and J. H. Bigelow, *Motivated Metamodels - Synthesis of Cause-Effect Reasoning and Statistical Metamodeling (MR-1570-AF)*. 2003.
- [62] Y. Jin, “Surrogate-assisted evolutionary computation: Recent advances and future challenges,” *Swarm Evol. Comput.*, 2011, doi: 10.1016/j.swevo.2011.05.001.
- [63] M. J. Asher, B. F. W. Croke, A. J. Jakeman, and L. J. M. Peeters, “A review of surrogate models and their application to groundwater modeling,” *Water Resour. Res.*, 2015, doi: 10.1002/2015WR016967.
- [64] E. Laloy and D. Jacques, “Emulation of CPU-demanding reactive transport models: a comparison of Gaussian processes, polynomial chaos expansion, and deep neural networks,” *Comput. Geosci.*, 2019, doi: 10.1007/s10596-019-09875-y.
- [65] M. T. Hagan, H. B. Demuth, and M. H. Beale, “Neural Network Design,” *Bost. Massachusetts PWS*, 1995, doi: 10.1007/1-84628-303-5.
- [66] J. Jatnieks, M. De Lucia, D. Dransch, and M. Sips, “Data-driven Surrogate Model Approach for Improving the Performance of Reactive Transport Simulations,” 2016, doi: 10.1016/j.egypro.2016.10.047.
- [67] M. De Lucia, T. Kempka, J. Jatnieks, and M. Kühn, “Integrating surrogate models into subsurface simulation framework allows computation of complex reactive transport scenarios,” 2017, doi: 10.1016/j.egypro.2017.08.200.
- [68] A. M. M. Leal, D. A. Kulik, and M. O. Saar, “Ultra-Fast Reactive Transport Simulations When Chemical Reactions Meet Machine Learning: Chemical Equilibrium,” *arXiv*. 2017.
- [69] D. Guérillot and J. Bruyelle, “Geochemical equilibrium determination using an artificial neural network in compositional reservoir flow simulation,” *Comput. Geosci.*, 2020, doi: 10.1007/s10596-019-09861-4.
- [70] C. Shen *et al.*, “HESS Opinions: Incubating deep-learning-powered hydrologic science advances as a community,” *Hydrol. Earth Syst. Sci.*, 2018, doi: 10.5194/hess-22-5639-2018.
- [71] A. M. M. Leal, D. A. Kulik, W. R. Smith, and M. O. Saar, “An overview of computational methods for chemical equilibrium and kinetic calculations for geochemical and reactive transport modeling,” 2017, doi: 10.1515/pac-2016-1107.
- [72] M. De Lucia and M. Kühn, “DecTree v1.0 – Chemistry speedup in reactive transport simulations: purely data-driven and physics-based surrogates,” *Geosci. Model Dev. Discuss.*, no. March, pp. 1–26, 2021, doi: 10.5194/gmd-

2020-445.

- [73] Y. Huang, H. Shao, E. Wieland, O. Kolditz, and G. Kosakowski, “A new approach to coupled two-phase reactive transport simulation for long-term degradation of concrete,” *Constr. Build. Mater.*, 2018, doi: 10.1016/j.conbuildmat.2018.09.114.
- [74] Y. Huang, H. Shao, E. Wieland, O. Kolditz, and G. Kosakowski, “Two-phase transport in a cemented waste package considering spatio-temporal evolution of chemical conditions,” *npj Mater. Degrad.*, vol. 5, no. 1, pp. 1–14, 2021, doi: 10.1038/s41529-021-00150-z.
- [75] D. Jacques, J. Perko, S. Seetharam, and D. Mallants, “Model abstraction addressing long-term simulations of chemical degradation of large-scale concrete structures,” *1 st Int. Symp. Cem. Mater. Nucl. Wastes*, no. October, pp. 11–13, 2011.
- [76] R. J. Millington and J. P. Quirk, “Permeability of porous solids,” *Trans. Faraday Soc.*, vol. 57, 1961, doi: 10.1039/TF9615701200.
- [77] E. Samson and J. Marchand, “Modeling the transport of ions in unsaturated cement-based materials,” *Comput. Struct.*, vol. 85, no. 23–24, pp. 1740–1756, Dec. 2007, doi: 10.1016/j.compstruc.2007.04.008.
- [78] J. F. Águila *et al.*, “Modeling cesium migration through Opalinus clay: a benchmark for single- and multi-species sorption-diffusion models,” doi: 10.1007/s10596-021-10050-5/Published.
- [79] M. Birgersson, L. Zheng, J. Samper, A. Mon, and L. Montenegro, “Arbeitsbericht NAB 16-23,” 2018.
- [80] J. Samper, A. Mon, and L. Montenegro, “A revisited thermal, hydrodynamic, chemical and mechanical model of compacted bentonite for the entire duration of the FEBEX in situ test,” *Appl. Clay Sci.*, vol. 160, pp. 58–70, Aug. 2018, doi: 10.1016/J.CLAY.2018.02.019.
- [81] C. Lu, “Reactive transport models in nuclear waste disposal and acid mine drainage,” Universidade da Coruña, 2009.
- [82] Q. Y. and L. Z. Samper, J., C Yang , L Montenegro, M Bonilla, C Lu, “Mass and energy balance and flux calculations for radionuclide release and geochemical evolution for SF carbon steel HLW repositories in clay and granite. Deliverable D-N°:5.1.13 of NFPRO project.,” 2007.